AIAA SciTech
5-9 January 2015, Kissimmee, Florida
56th AIAA/ASCE/AHS/ASC Structures, Structural Dynamics, and Materials Conference

for Challenges in the Design of Joined Wings Special Session

PrandtlPlane Joined Wing: Body Freedom Flutter, Limit Cycle Oscillation and Freeplay Studies

Rauno Cavallaro*, Rocco Bombardieri†, Luciano Demasi‡, Andrea Iannelli§

Dynamic aeroelastic behaviour of a joined-wing *PrandtlPlane* configuration is here investigated. The baseline model is obtained from a configuration previously designed by partner Universities through several multi disciplinary optimizations and several ad-hoc analyses, including also detailed studies on the layout of control architecture. This represented an ideal starting point since, due to the novel design, realistic layout of the mobile surfaces, stiffness and inertia distributions are not available nor easily determinable. An equivalent structural model has then been adopted to qualitatively retain similar aeroelastic properties with great benefits for the applicability of results.

Flutter and post-flutter regimes, including limit cycle oscillations (LCOs) are studied. A detailed analysis of the energy transfer between fluid and structure is carried out and the areas in which energy is extracted from the fluid are identified, to gain insights on the mechanism leading to the aeroelastic instability.

Starting from an existing design of mobile surfaces on the baseline configuration, freeplay is considered and its effects on the aeroelastic stability properties of the system are investigated.

Both cantilever and free flying configurations are analyzed. Fuselage inertial effects are modeled and the aeroelastic properties studied considering plunging and pitching rigid body modes. For this configuration a positive interaction between elastic and rigid body modes turns the design in a flutter free one (in the range of considered speeds).

To understand the sensitivity of the system and gain insight, fuselage mass and moment of inertia are selectively varied. For a fixed pitching moment of inertia, larger fuselage mass favours the body freedom flutter. When the moment of inertia is varied, a change of critical properties is observed. For smaller values the pitching mode becomes unstable, and coalescence is observed between pitching and first elastic modes. Increasing pitching inertia, the above criticality is posticipated and, in the meanwhile, second elastic mode becomes unstable at progressively lower speeds. For larger inertial values "cantilever" flutter properties, having coalescence of first and second elastic modes, are recovered.

I. Introduction

It is a recurring circumstance, in aircraft design, to re-size layout after a preliminary assessment of a solution outcome of a conceptual design stage. For cantilever classical configurations, after years of practice and experience this problem has been mitigated and does not represent an insurmountable issue. For Joined Wings there is no similar industrial experience. Thus, attempts to conceptually design such a configuration using handbook or very low fidelity tools have always resulted in non-competitive layouts. For example, using standard structural design tools calibrated on traditional configurations may lead to considerably heavier configurations than a reference optimized traditional one, with *consequent non-demonstrated claims about non-competitiveness* of the joined-wing aicraft. An interesting discussion about the need of an ad-hoc design practice in order to exploit the potential benefits is given in Refs. [1, 2]. However, the situation is actually

*PhD, Department of Aerospace Engineering, San Diego State University and Department of Structural Engineering, University of California San Diego, AIAA Member
†Visiting Graduate Student, San Diego State University, MS Candidate at the Dipartimento di Ingegneria Aerospaziale, Università di Pisa
‡Associate Professor, Department of Aerospace Engineering, San Diego State University, AIAA Senior Lifetime Member
§MS, Dipartimento di Ingegneria Aerospaziale, Università di Pisa.

even more challenging. Due to the geometrical layout of a typical Joined Wing, there is an unavoidable coupling of the different disciplines. Being this true also for traditional configurations, for Joined Wings this is pushed to the limit. For example, the flight mechanics requirements on low speed conditions may not be completely satisfied with a fine-tuning of the flap/slats design, and this constraint may completely change the layout in terms of twist distribution and sweep angle. In other words, a multidisciplinary optimization seems to be unavoidable. An example of *PrandtlPlane* applied optimization process (although structural constraints were not considered) is presented in Refs. [3, 4].

One of the major challenges in the design of Joined Wings is represented by important structural nonlinearities which are significant even at very low incidence and attached (linear) flow. Moreover, as already shown in the literature [5–9] the typical joined-wing layout, featuring an overconstrained system at global level, is responsible of introducing strong structural nonlinearities and counterintuitive behaviors. This high complexity implies that at early design phases of the configuration, even adopting a multidisciplinary optimization, but relying on linear tools, may lead to far-from-optimal or even impossible-to-fly configurations.

Several theoretical studies [10–14] tried to address this difficulty by employing reduced order models. However, their efficiency was found to be unsatisfactory.

Given this scenario, efforts to better understand possible problems of geometrical nonlinearities at structural level were made [7–9, 15]. The results were obtained on conceptual wind-tunnel-like models, and snap-types of instabilities were observed. Aeroelastic static analyses showed that eigenvalue approach for aeroelastic divergence speed assessment was overpredicting the true instability speed. In Ref. [16, 17] nonlinear aeroelastic dynamic responses were shown: not only the *true* critical speed was found to be lower than the one predicted considering the undeformed structure, but several phenomena as flip-bifurcation, multi-stability and eventually chaos were observed. When a source of *nonlinearity* of aerodynamic origin (wake roll-up) was incorporated, the effects were noticeable.

Natural extension of these efforts is to apply the gained knowledge and the in-house computational tools to study the nonlinear aeroelastic response of a more *realistic* layout, obtained through preliminary optimization and fine-tuning, as the ones presented in Refs. [18–21]. This design features a commercial aircraft application and thus, differently than previously investigated cases, is characterized by smaller displacements.

II. Contribution of the Present Study

Considering the literature on design of Joined Wings, with emphasis on *Box Wing* [22] and *PrandtlPlane* [23–25] configurations, a significant amount of work has been carried out, see for example Ref. [26]. Thus, a *realistic* reference configuration based on these works is available for thorough aeroelastic analysis: it is well known [27, 28] that the stiffness and inertial distributions play a primary role in the occurrence of flutter.

More in details, this paper will feature a *PrandtlPlane* layout *similar* to the one studied in Refs. [18–21]. This model was obtained through a partial MDO and then progressively fine-tuned [26, 29–32].

Given also the studies on *flight mechanics* and control surfaces [20, 21], this configuration represents an interesting starting point for studying nonlinear aeroelasticity and freeplay effects. *Impact of control surface freeplay on flutter* [33, 34] has never been studied before for Joined Wings. Differently than traditional configurations, for the PrandtlPlane Joined Wings there are multiple mobile surfaces located on both wings. Thus, the response of the system will be the result of a complicated interaction of each control surface freeplay. The contributions of this paper are outlined below.

- Starting from the joined-wing model presented in Ref. [18], a structurally "equivalent" model is designed. The mobile surfaces are considered being perfectly connected to the wing around the hinge line (no freeplay), and flutter analysis is carried out. However, a further step is taken: the post-flutter response is tracked with a time-domain capability, showing the limit cycle oscillation. Aerodynamic-structure energy transfer is also investigated and discussed.

- The second contribution, is on the impact of control surface freeplay on flutter response of this configuration. Mobile surfaces have been previously designed for this specific configuration complying with handling qualities requirements at various flight conditions, see Refs. [20, 21, 35] for details. Thanks to these efforts, and assuming a reasonable law describing a realistic freeplay of mobile surfaces, it is possible to study that effect on the aeroelastic response of the overconstrained system represented by the PrandtlPlane. This is carried out both on the frequency domain, in which the rigid modes associated with the free surfaces are interacting with the elastic modes changing flutter properties, and

on the time domain, where the nonlinear response of freeplay and its effects on limit cycle oscillation amplitude and frequency are observed.

- The flutter analysis are repeated when also rigid body modes are considered. In fact, in literature several Joined Wings presented low frequencies of the first natural modes (e.g., [18, 36, 37]), favouring a possible interaction between elastic and rigid modes. Other than pursuing such an investigation (commonly referred to as free-free or free-flying aeroelastic analysis), a sensitivity analysis is carried out by changing fuselage weight and (pitching) moment of inertia.

The present effort, based on a qualitatively *realistic* layout, is logically part of conceptual analyses [6, 8, 9, 15–17, 38]. Moreover, it represents a step towards a full trimmed (structurally) nonlinear aeroelastic analysis of the PrandtlPlane configuration, in which also freeplay effects of mobile surfaces are considered.

III. Theoretical Highlights Regarding the Present Computational Tool

The in-house computational capabilities are here briefly outlined. They consists in a finite element method for the computational solid dynamics (CSD), a doublet lattice method (DLM) for the frequency domain unsteady aerodynamic and an unsteady vortex lattice method (UVLM) for the time domain aerodynamics. The coupling (time integration) and interfacing (load and displacement transferring) are described in detail in Refs. [16, 17]. Briefly, an implicit integration scheme is used to advance in time, being the nonlinear problem at each time-step solved by means of a Newton approach. Moreover, the interface information is passed through *moving least squares* (MLS) approach.

It this interesting to point out that these tools are prospectively sufficient to capture the physics of the here sought phenomenon (see Ref. [16]). In fact, experimental and numerical works have clearly shown how, in many cases, the structural nonlinearities drive the limit cycle oscillation much more than the aerodynamic ones do. Ref. [34] showed a limit cycle oscillation on a wing in which freeplay was taken into account. When the numerical results were not in good agreement with the experiments, this was a consequence of the neglected structural geometric nonlinearities [39–41].

A brief description of the in-house capability is presented in the following.

A. Structural finite element model

The geometrically nonlinear finite element [42–45] is based on the linear membrane constant strain triangle (CST) and the flat triangular plate element (DKT). The capability has also embedded the calculation of the structural tangent matrix $\boldsymbol{K}_T$, which is sum of two contributions: the elastic stiffness matrix, $\boldsymbol{K}_E$, and the geometrical stiffness matrix, $\boldsymbol{K}_G$. Composite material composed of several and differently oriented layers (theoretically these layers could also be of different materials) are implemented. A corotational approach is used, and thus rigid body motion is eliminated from elements and the pure elastic rotations and strains are found.

In order to tackle the freeplay problem, and simulate the play of the control surfaces, the present computational tool was further added the capability of specifically modeling nonlinear springs. The ad-hoc formulation is briefly presented below. Multifreedom constraint (MFC) capability completes the set of the tools needed to properly model mobile surface devices behavior. Both the springs and the MFC give a contribution to the structural tangent matrix $\boldsymbol{K}_T$. The freeplay springs contribution is presented in detail in Appendix A.

For the free-free analysis, rod and lumped mass elements are needed to model rigid connections and concentrated masses located in the space to model fuselage inertial contributions. The first ones give a contribution to the tangent matrix, whereas the second ones contribute to the system's mass matrix.

1. Freeplay springs

A generic connection between two finite elements sharing a common part of the hinge line is presented in Fig. 1. Nodes H1 (H2) and H3 (H4) are connected through translational MFCs, which force them to be (almost) coincident in space. The "freeplay spring" is a rotational spring acting on the hinge line, reacting to relative rotations between the two elements (called for reference Master and Slave). Defining a direction on the hinge line, $\boldsymbol{e}^A$, the relative rotation $\Delta\theta$ can be measured, accordingly with the axis direction. This enables the evaluation of the moment exerted by the spring once the law $M(\Delta\theta)$ is defined. This moment

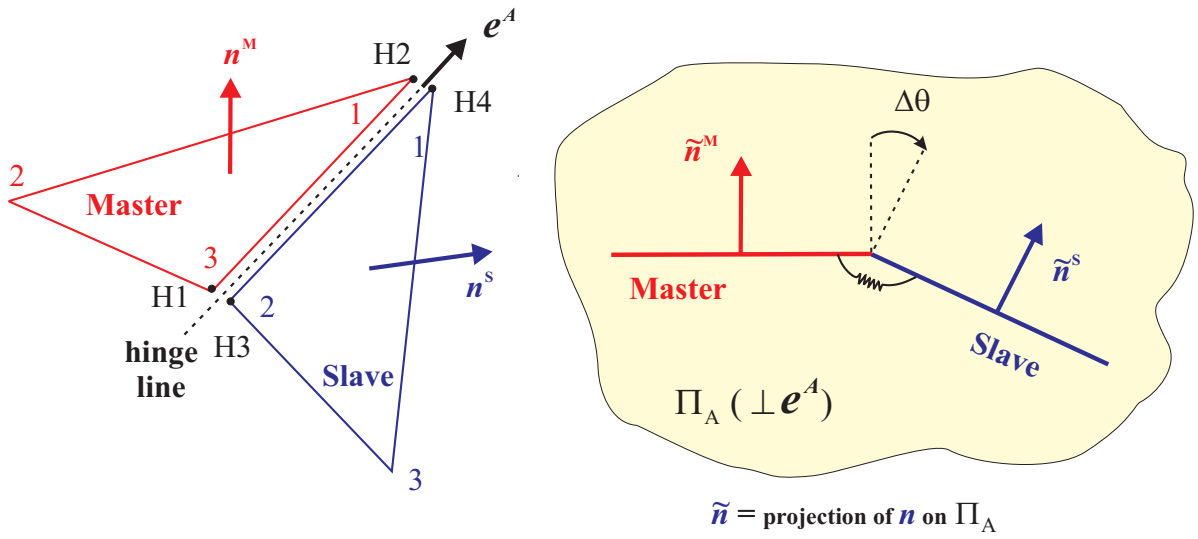

Fig. 1. Freeplay spring acting on the hingeline connecting two finite elements.

acts on the elements, with the appropriate sign: for the master element $\boldsymbol{M} = M(\Delta\theta)\, \boldsymbol{e}^A$, whereas for the slave the opposite holds.

Final step consists in projecting the rotational actions, thought on the hinge line, on the hinge nodes. This is simply accomplished by equally distributing the moment between the nodes. Summarizing:

$$\begin{cases} \boldsymbol{M}^{H1} = -\dfrac{\boldsymbol{M}}{2} & \boldsymbol{M}^{H2} = -\dfrac{\boldsymbol{M}}{2} \\ \boldsymbol{M}^{H3} = \dfrac{\boldsymbol{M}}{2} & \boldsymbol{M}^{H4} = \dfrac{\boldsymbol{M}}{2} \end{cases} \tag{1}$$

where $\boldsymbol{M} = M(\Delta\theta)\, \boldsymbol{e}^A$.

As said, angle $\Delta\theta$ is the relative rotation of the two elements along the hinge line, and thus is evaluated in the perpendicular plane $\boldsymbol{\Pi}_A$. Then, the relative rotation can be expressed (in radiants) as:

$$\Delta\theta = \sin^{-1}((\boldsymbol{n}^M \times \boldsymbol{n}^S) \cdot \boldsymbol{e}^A) \tag{2}$$

where $\boldsymbol{n}^M$ and $\boldsymbol{n}^S$ are the normals of the master and slave element, respectively. This equation is representative of the relative rotation about the hinge line.

Freeplay affects directly the law relating the reaction moment and the relative angle. A mobile surface freeplay could be reproduced using a piecewise value of the spring stiffness K_θ (which could ideally represents the reaction of aileron actuator). As shown in Fig. 2, it exists a region delimited by the angle 2δ in which the aileron is free to rotate. Outside of this region the spring (actuator) has a non-zero stiffness. For a numerical point of view, however, it may not be convenient to use such a description, since it does not fit well solution strategies based on Newton's iterations. On the contrary, continuity of the derivative (spring stiffness) has been guaranteed smoothly connecting the different value with one of the several options described in the literature. In particular, Fig. 3 shows the smoothed law, when a sigmoid-like function is used to approximate the derivative. Small numerical timesteps are needed to guarantee convergence. A more robust and less computationally demanding approach is outlined in [46].

B. Aerodynamic models

The computational tools used for the evaluation of the aerodynamic forces are based on the hypothesis of potential flow (non-viscid and irrotational). As said before, the interest of this effort is to evaluate the effect

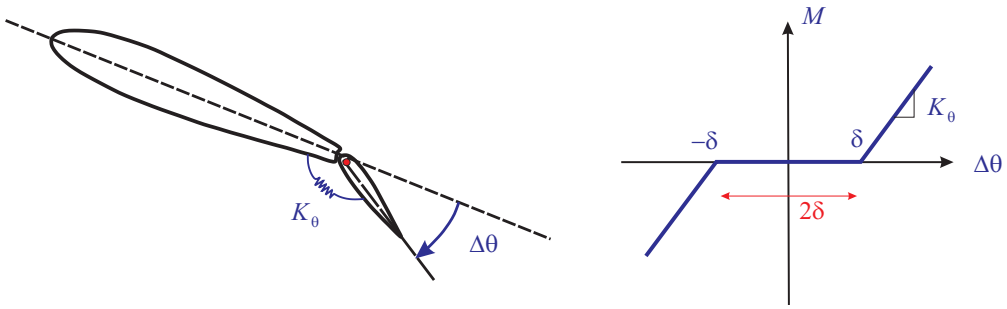

Fig. 2. Freeplay concept: in the region delimited by the angle δ the surface is free to move without encountering any resistance.

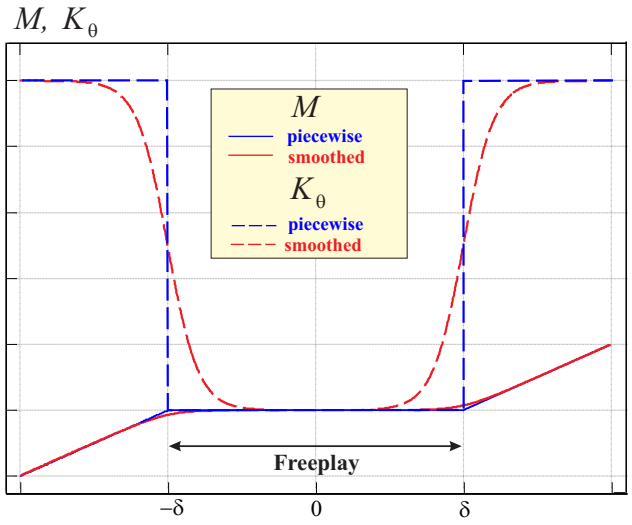

Fig. 3. Smoothed piecewise freeplay law.

of the structural nonlinearities, thus, complicated nonlinear aerodynamic phenomena such as shockwave-boundary layer interaction, flow separation, etc, are not considered. Considering the hypothesis of attached flow the potential flow theory underlying the computational method is adequate to simulate the aerodynamic field with very low computational costs.

For the flutter speed prediction a frequency domain unsteady aerodynamic model (the Doublet Lattice Method, DLM [47]) is used. For the time domain simulations, necessary to simulate the evolution of the aeroelastic system, an unsteady vortex lattice method (UVLM) (see [48]) is adopted. The in-house capability has also built-in the aerodynamic tangent matrix $\boldsymbol{K}_A$, which is useful when using an implicit time-integration approach. For more details the reader is referred to following efforts: [9, 15–17].

As far as load and displacement transfers are considered, an *MLS* approach is chosen [49]. In this way, it is possible to project a force acting on the aerodynamic grid onto the structural one, and vice versâ, project the displacements (deformations) of the structural grid onto the aerodynamic ones. A more thorough treatise on this topic is also shown in [17].

IV. Description of the Analyzed *PrandtlPlane* Configuration

The chosen configuration is a typical *PrandtlPlane*, an artistic view is given in Fig. 4 (reproduction from Ref. [19]). It is a 250 passenger mid-long range (6000 nm) design with a MTOW of 230 tons. It will be addressed throughout this section with the name *PrP250*. The external surface and general layout shape were designed also with the aid of an MDO software, presented in Refs. [3, 4]. Later, the structures were fine-tuned [19, 29] taking into account different constraints as maximum stress, local buckling of stiffened panels, aileron efficiency, static aeroelasticity and flutter. The structural model used for linear flutter analysis

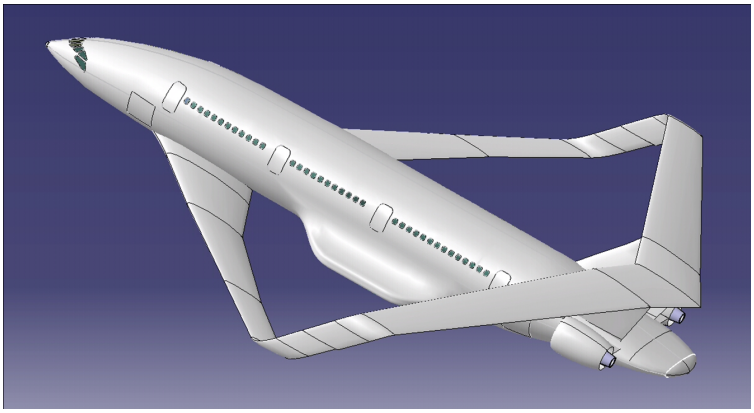

Fig. 4. Artistic view of the *PrP250*, taken from [19].

is shown in Fig. 5.

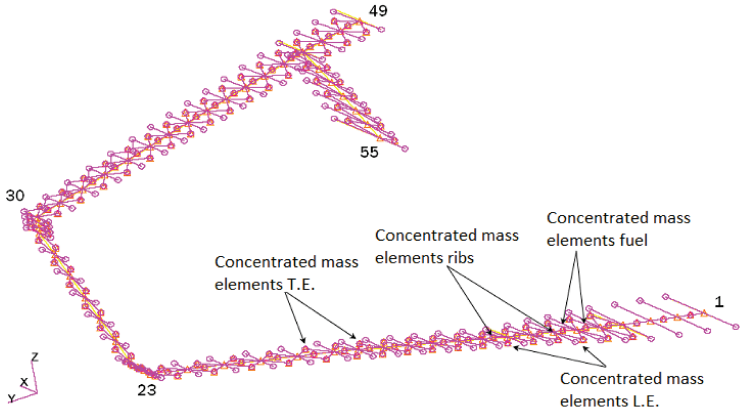

Fig. 5. Structural model used for flutter analysis of *PrP250*. Taken from [19].

Further work has been carried out optimizing the structure and, finally, employing composite materials [31, 32], although in the present work the focus will be the one built with *aluminium alloy*. Flutter analysis was also the focus of parallel works [18, 30].

The mobile surfaces have been sized in Refs. [20, 21, 35]. An excerpt of the layout is shown in Fig. 6. According to these last references, the design of the flight controls was complying with a set of handling qualities requirements at various flight conditions (low speed, high speed, crosswind, high altitude and low altitude). The handling qualities requirements were involving maneuvers as push pull, minimum time to bank, aircraft trim with one engine out, take-off rotation and steady turn. A linear stability analysis indicated that the aircraft had good longitudinal handling qualities and was stable. Moreover, the aircraft configuration made it possible to have pure torque control in pitch.

A. Baseline model

1. Equivalence process

Since the original structural configuration was modeled with beam elements first, and later a detailed full wing-box model was designed (as shown in Ref. [31]), and since the focus of the present effort is towards a conceptual work, it has been decided to build an "equivalent" shell structure describing only a medium surface. In order to match the properties of the structures in terms of modes, different preliminary approaches have been investigated. In particular, the following options have been explored:

- equivalent model through analytical static stiffness approach and dynamic mass equivalence;

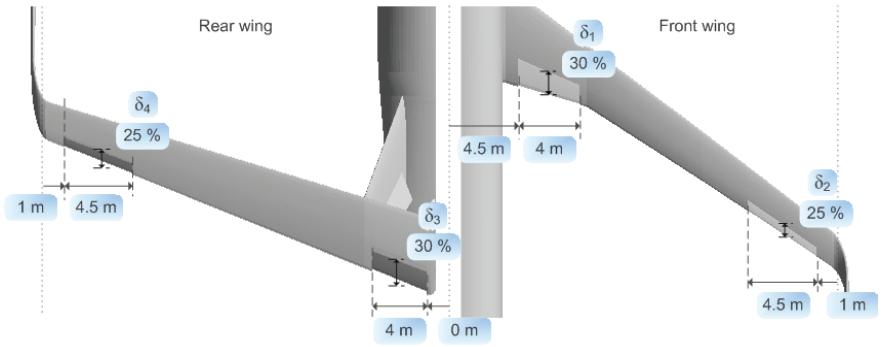

Fig. 6. Control surfaces layout for *PrP250*. Taken from [20].

- modal equivalence following the process shown in Ref. [50];
- modal equivalence through an optimization process.

The last approach has been proven to be the most successful. The inherent overconstrained nature of the system has put a remarkable difficulty in the matching process, consequence of the coupling of primary bending, torsion and secondary bending, with the consequence that the modes were all showing, at different extent, some level of deformations inherent to the above described features.

Although slightly different, aeroelastic scaling shares commonalities with the present problem. It was pursued in literature in different efforts, and did show to be an unexpectedly difficult task to be accomplished on Joined Wings, see for example Refs. [51, 52].

The first natural modes of the beam model were considered. By means of an extrapolation, the target mode shapes were obtained for the surface described by shell elements. Some physical reasoning suggested to use a multi-layer structure, in which the different layers' fibers were oriented perpendicularly to each other in order to easier decouple, for example, the bending and torsional effects. In particular, after testing different solutions, a five-layer laminate, with a $0/90/0/90/0^\circ$ (the local direction about which the angle were measured was the axis of the beam model) pattern was employed: the second and fourth layer were *mainly* regulating the torsional stiffness, the ones on the sides were *mainly* controlling the bending stiffness, whereas the central layer had most of the impact in *fine tuning* the extensional stiffness. This choice was also confirmed to be an appropriate one with preliminary numerical experiments carried out for validation purposes on simpler wing layouts.

The structure has been then divided in 23 different segments, each of which had a direct correspondence to the different geometrical segments of the real wing (kink, different dihedral, joint, fin, etc...). For each segment, layers' material properties as well as thickness and density were chosen as the design variables. The objective function to be minimized was containing a mismatch on the natural frequencies. Moreover, the minimization process had some inequality constraints on the thicknesses and density of the layers. This has proven to be a quite successful approach, within the limit set by the different physical models.

Within the optimization approach, different methodologies were tested. Initially, a global optimization process (based on work [53]) was tested, with the local optimization carried out with the tools offered by the commercial software *Matlab Optimization Toolbox*. However, due to the large required computational resources (caused by the model complexity), it was chosen to run a local optimization process, starting from a reasonable configuration found with previous equivalence procedures (see above) as "first guess".

A crucial step was the capability of correctly associate the modes with the target ones for correct identification of the frequencies to be used for the objective function.

Matching was carried out for the first 5 modes only. This choices was consequence of the following facts:

- Optimization process was time consuming. More design variables were eventually needed for reasonable matching with higher frequency modes, with a relevant increase in the costs of the optimization process.
- The overall sense of the equivalence was in giving a more realistic stiffness and distribution mass, rather than perfectly matching a structure, like the beam one, which is inherently not the "exact" model.

Matching the first five modes was not a trivial problem. After several numerical tests it was found that the "best" fitting was obtained by relaxation of the matching of the fourth mode. Summarizing, the following results were achieved in terms of mismatch on the natural frequencies of the modes:

0.02%	first mode
5.06%	second mode
0.01%	third mode
24.33%	fourth mode
0.87%	fifth mode

Results showed that the laminate where all presenting symmetric layup, giving credit to the initial assumptions on the fibers' direction.

The matching was pursued on the structure without the fuel. This configuration represented the departure moment from the original beam model of [30] and the authors made different choices. For example, the fuel was uniformly distributed on the structural (coincident with the aerodynamic) surface, in particular on the two wings, and not on the joint and vertical empennage. With uniform, the authors mean that an equivalent surface density was used to match the same quantity of fuel allocated in the different wing segments. For the beam model the fuel was allocated slightly behind the elastic beam axis. This certainly affects flutter occurrence and nature. However, as already stated, the aim of this research is *not to reproduce the exact flutter scenario* of the reference model, but to use its geometry, stiffness and mass distribution as a starting point and later perform *conceptual* investigations.

Although the first five modes were thought to dynamically (not necessarily from an aeroelastic point of view) retain most of the physics, this was not the case for the static point of view. A small mismatch on tip deflection for a mechanical pressure load was observed. The material stiffness and density were slightly scaled, conserving thus the same modal properties, and pursuing thus a better static matching. As a consequence, the total mass of the original model was restored (within limits) by scaling the total amount of allocatable fuel.

In order to better reproduce loss in stiffness consequence of the mobile surface presence without modeling any sort of freeplay, the model was "cut" in correspondence of lateral edges of mobile surfaces. Moreover, the fuel mass was not distributed on the mobile areas, as will be better explained in the next section. In other words, this model had control surfaces perfectly clamped on the theoretical hinge line.

Hereinafter, the configuration obtained with the equivalence process outlined above will be considered as the *baseline configuration*.

2. Constraints

First let us introduce the coordinate system. x is directed along the streamwise direction and z vertically. $y = 0$ (plane xz) represents a symmetry plane.

Sections on the symmetry plane are allowed to translate in the plane, and rotate perpendicularly to it. Root section of the fin is clamped. The section slightly inboard of the elevator on the front wing where ideally intersection with the fuselage take place is only free to rotate in the stream direction x.

B. Mobile surfaces

Mobile surfaces had to be modeled in order to study freeplay effects. This was done following works presented in Refs. [20,21,35]. Since cutting the mobile surfaces intuitively implies a change of the stiffness properties, it was checked that this process was not significantly changing the natural frequencies and also the flutter speed and properties of the model. The mobile surface's mass was set unloading it from the fuel part (diminishing the density of the material). Actually, also the option of regulating their weight with handbook procedures, as shown in [54] was explored. Once again, use of such tools on a unconventional configuration is strongly debatable, and is here justified by the conceptual character of this effort.

Location of mobile surfaces, as designed in Fig. 6, are pictorially shown in Fig. 7. In the following of this section, the model in which the mobile surfaces are designed are identified with 5 digits string, being each digit 0 or 1 whether the surface is perfectly constrained or not, and following the sequence: front elevator, front aileron, rear aileron, rear elevator and rudder. For example, 01010 refers to a configuration with fixed front elevator, rear aileron and rudder.

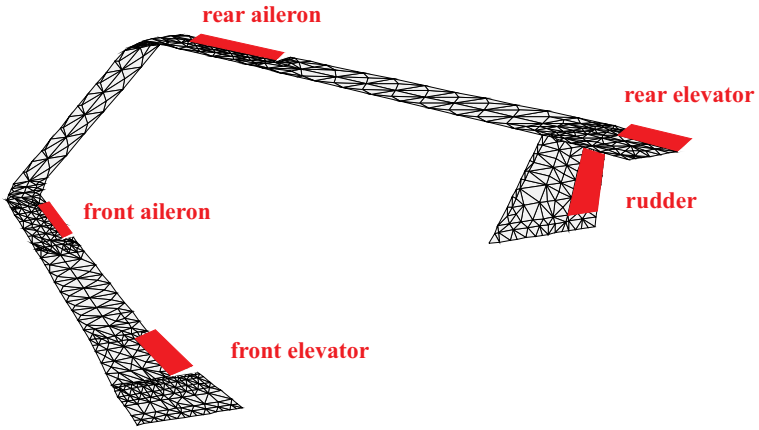

Fig. 7. Location of control surfaces.

V. Flutter Properties of the PrandtlPlane

Flutter analysis has been carried out on *PrP250*. As explained, the control surfaces have been considered perfectly-rigidly connected (clamped) to their upstream wing-part. The frequency domain in-house code, based on *DLM* and root-locus technique [17] has been validated against the commercial code *NASTRAN*. The nominal aerodynamic and structural meshes are represented in Fig. 8. The choice of the discretization was driven by convergence analysis: the in-house finite element capability has proven to be converged with the mesh shown in the picture, whereas a little more refined model (non depicted in the figure) was needed for *NASTRAN* in order to achieve convergence.

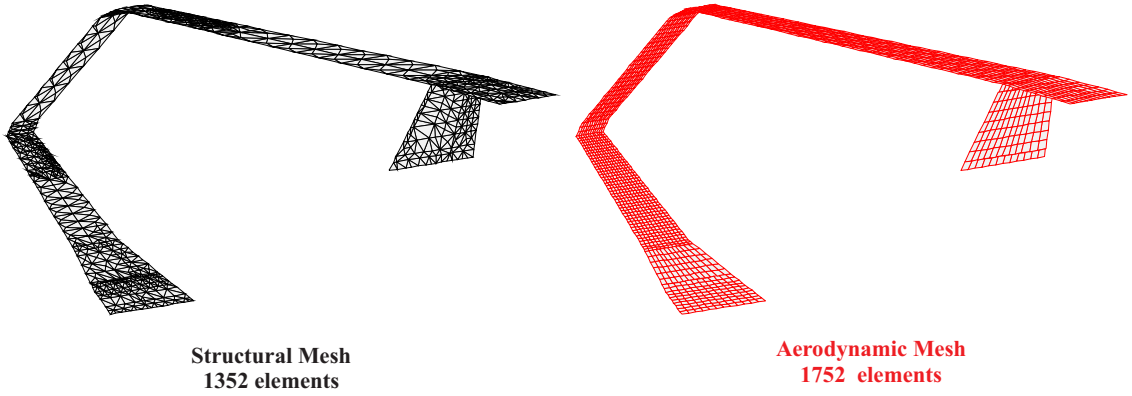

Fig. 8. Nominal structural and aerodynamic meshes used for the aeroelastic analysis.

The first five natural modes and associated frequencies are represented in Fig. 9. Due to the over-constrained nature of the layout bending/torsion coupling of both wings is enhanced. The *first mode* is characterized by a vertical deflection of the wings, with an (almost) rigid vertical translation of the joint. Having the wings almost opposite sweep angle values, and being connected trough the joint, a complicated torsional deformation can be observed. In the *second mode* the joint tilting is dominating the deformation, inducing the characteristic wing bending and torsion. Moreover, the joint itself bends. On the contrary, in the *third mode* the joint (almost) rigidly translates horizontally and vertically and slightly tilts inward/outward. The *fourth* mode has a prominent torsional deformation of the joint. *Fifth mode* resembles the second one, however, for a very similar joint displacement and deformation, opposite wing bending are present. In particular, the lower wing presents a more complex bending deformation when compared to mode II.

The frequencies of the modes are not high, and this suggests that interaction with rigid body motion can be non-neglibile. This will be investigated in a dedicated section of this effort (namely section VII), however, for the moment, the fixed (cantilever) system is considered.

Results of flutter analysis are shown in Figs. 10 and 11 in terms of real and imaginary part of the

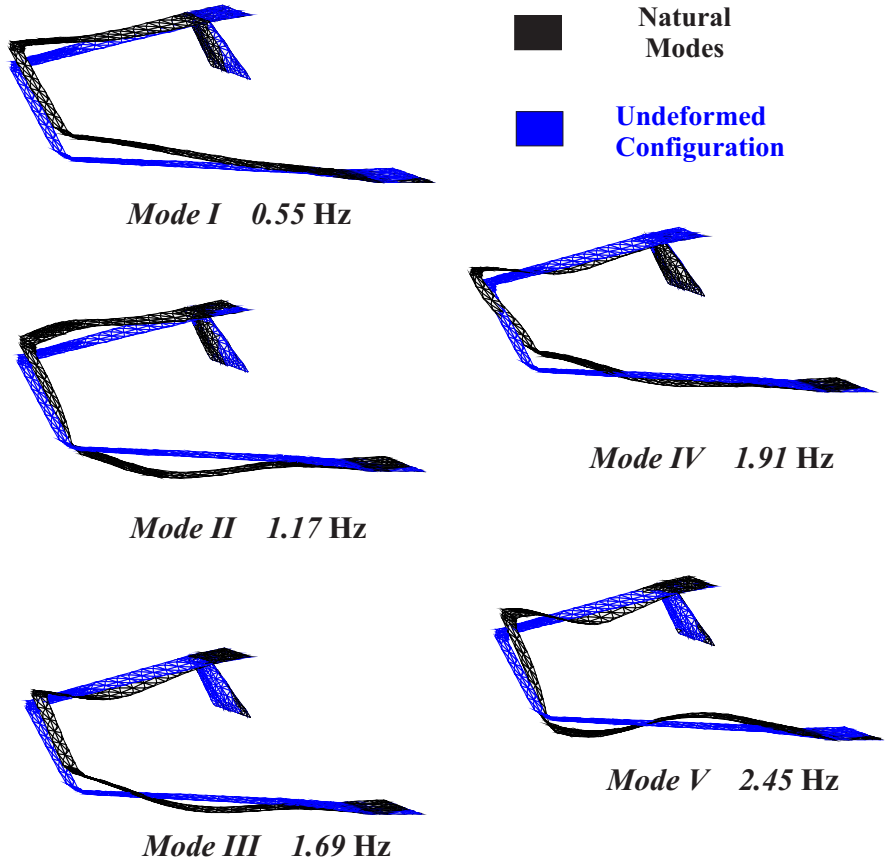

Fig. 9. First five natural modes and associated frequencies.

eigenvalues of the system for different wind speeds. How it can be easily inferred, the second mode becomes unstable (flutter) for a speed of approximately 257 m/s. Moreover, coalescence of the frequencies of the first two modes is observed before flutter occurs. The associated root locus is shown Fig. 11.

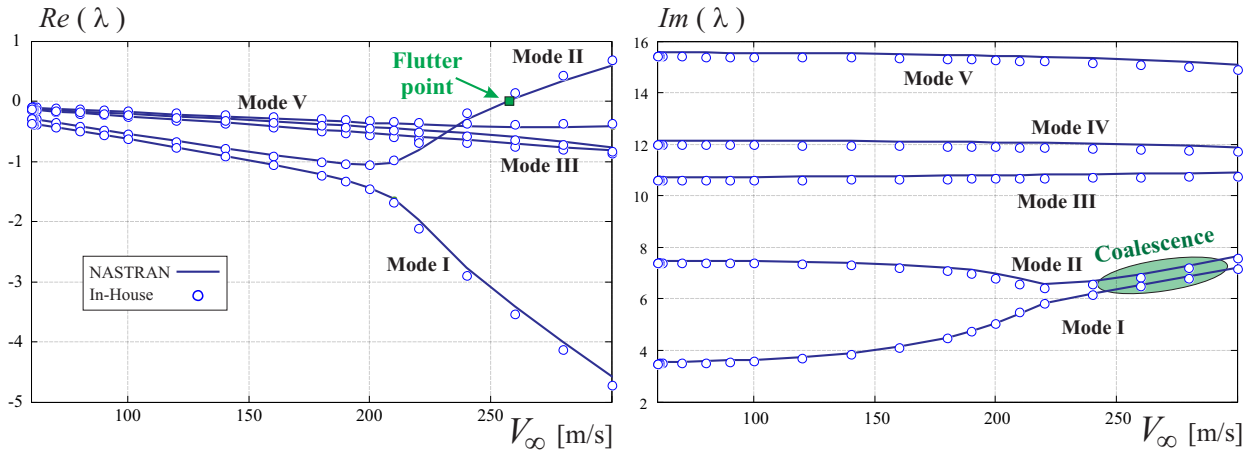

Fig. 10. Real and Imaginary parts of the eigenvalue of the system at different speeds.

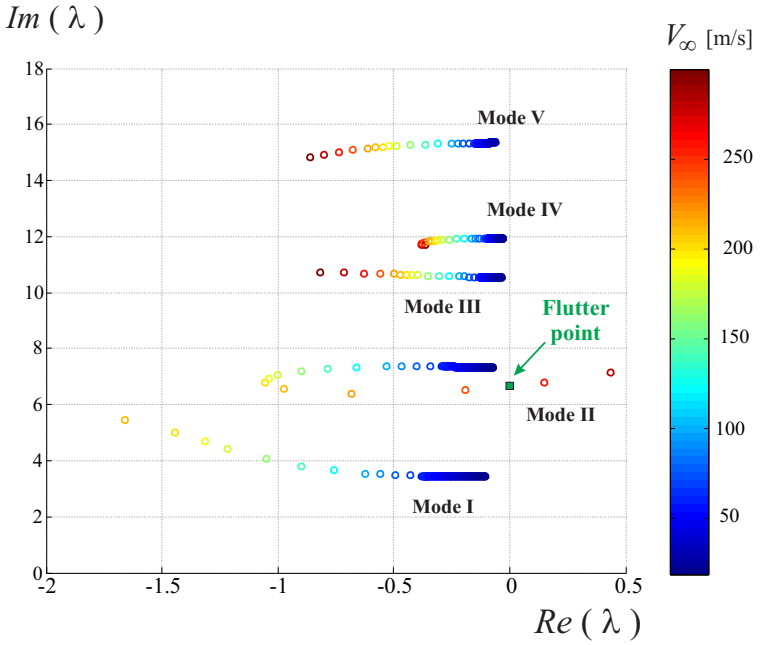

Fig. 11. Root locus of the system. The different colors identify the associated speed.

A. Time domain analysis and energy transferring

A nonlinear dynamic aeroelastic analysis is performed at the speed of 260 m/s, which is a post-flutter regime. The undeformed configuration is considered, and a vanishing perturbation in angle of attack is given to accelerate the transition to the limit cycle oscillation. Note that the previous flutter analysis was performed using the modes at the undeformed state; thus it is expected that including structural nonlinearities changes the flutter point with respect to Fig. 10; also please note that this is not a matched flutter analysis for simplicity of the theoretical conceptual discussion.

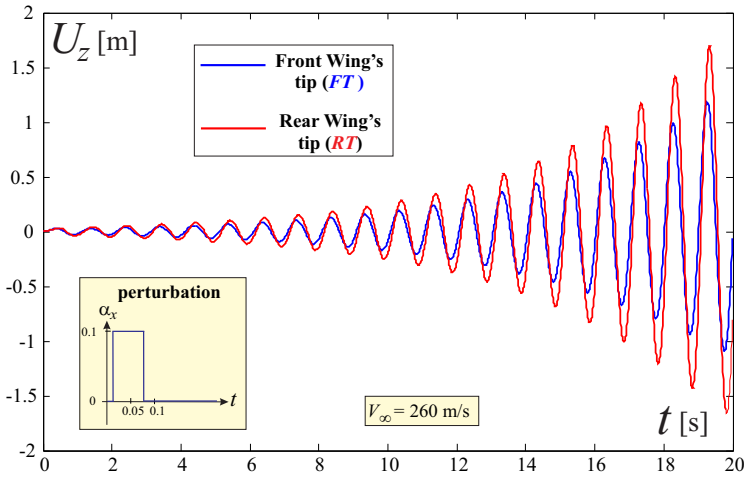

Fig. 12. Time response of the system for $V_\infty = 260$ m/s: vertical displacement of the lower (FT) and upper (RT) wing's tip.

The response for the lower and upper wing's tip (named FT and RT) is presented in Fig. 12. If the deformed configurations are plotted within a wave (between time 16 s and 17.1 s), the pattern shows (see Fig. 13) that the deformation resembles mainly a superposition of the first and second natural modes. Interestingly enough, the first and second modes are also the ones that coalesce for a wide range of speeds relatively close to the flutter one. In Fig. 13 it is possible to observe a shorter or longer joint. However, this

graphical representation is only a projection of the joint and the change in length is mainly due to a rigid rotation (tilting).

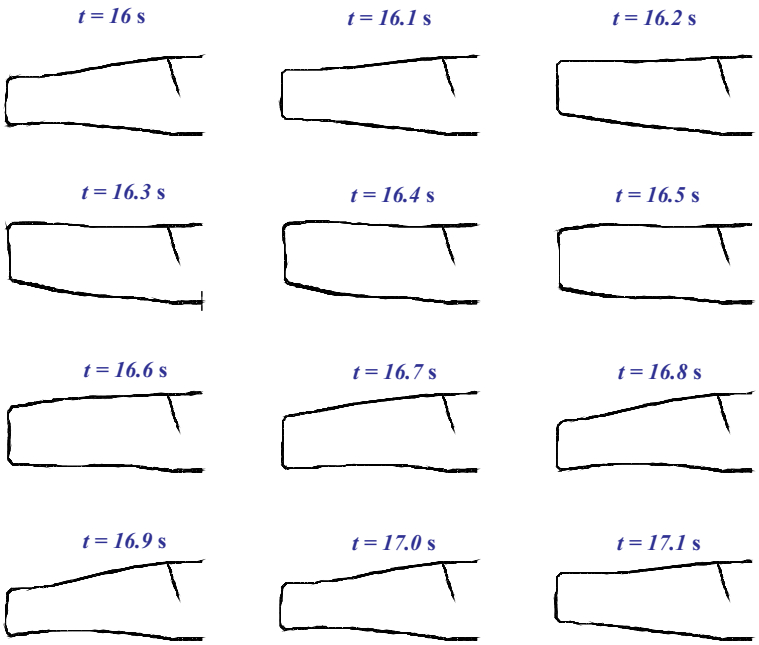

Fig. 13. Time response of the system for $V_\infty = 260$ m/s: magnified (2x) deformations at different snapshots taken in the interval $16 \div 17.1$ s.

In Fig. 14, successive plots of the deformed configuration colored according to the *power of the aerodynamic forces* are shown within the same time window. When the power is positive (negative) fluid is transferring (extracting) energy to (from) the structure. Being the response preceding a LCO a positive quantity of energy is absorbed by the structure in one cycle. However, it is interesting to observe that lower wing almost always extracts energy, whereas different parts of the upper wing alternate between transferring and absorbing.

B. Post-flutter response and LCO

Focus is now on the limit cycle oscillation that develops after the transient has elapsed. A procedure similar to the one proposed above is here again used, at the same wind speed of 260 m/s. In Fig. 15 the time-displacement of the lower and upper wing's tip are depicted. Moreover, to better characterize the LCO, also the phase spaces are shown. The displacements and velocities are larger for rear wing's tip.

Effects of modeled wake's length In all above cases, wake was modeled without allowing for roll-up. Although in some case in literature this has been shown to have a non-negligible impact on aeroelastic response (see Refs. [16,17]), it is generally a widely used an well accepted approximation. Within a boundary element approach (BEM), modeling of the wake may be computationally intense for unsteady simulations. In particular, without a free wake modeling is important to keep the timestep constant in order to avoid to recalculate the aerodynamic influence coefficients of the wake. On the other hand, time step needs to be small enough to appropriately track the unsteady phenomena and avoid convergence problems (in nonlinear approaches).

In literature a wake's length of about 20 times a reference value (usually the wing's chord) was showing converged results (in terms of steady forces), see for example Ref. [55]. However, considering computational costs, the authors did a preliminary analysis with the aim of reducing wake's length while retaining the aeroelastic transient and asymptotic behaviour. Wake's length slightly larger than ten times a reference dimension (root chord), was proven to be enough.

The following simulation limits wake's length to a very short value (slightly larger than the chord reference), with the spirit of observing the different aeroelastic behavior. As depicted in Fig. 16, when a very short wake is modeled, time to reach the LCO is larger, its amplitude and frequency are smaller. Wake carries

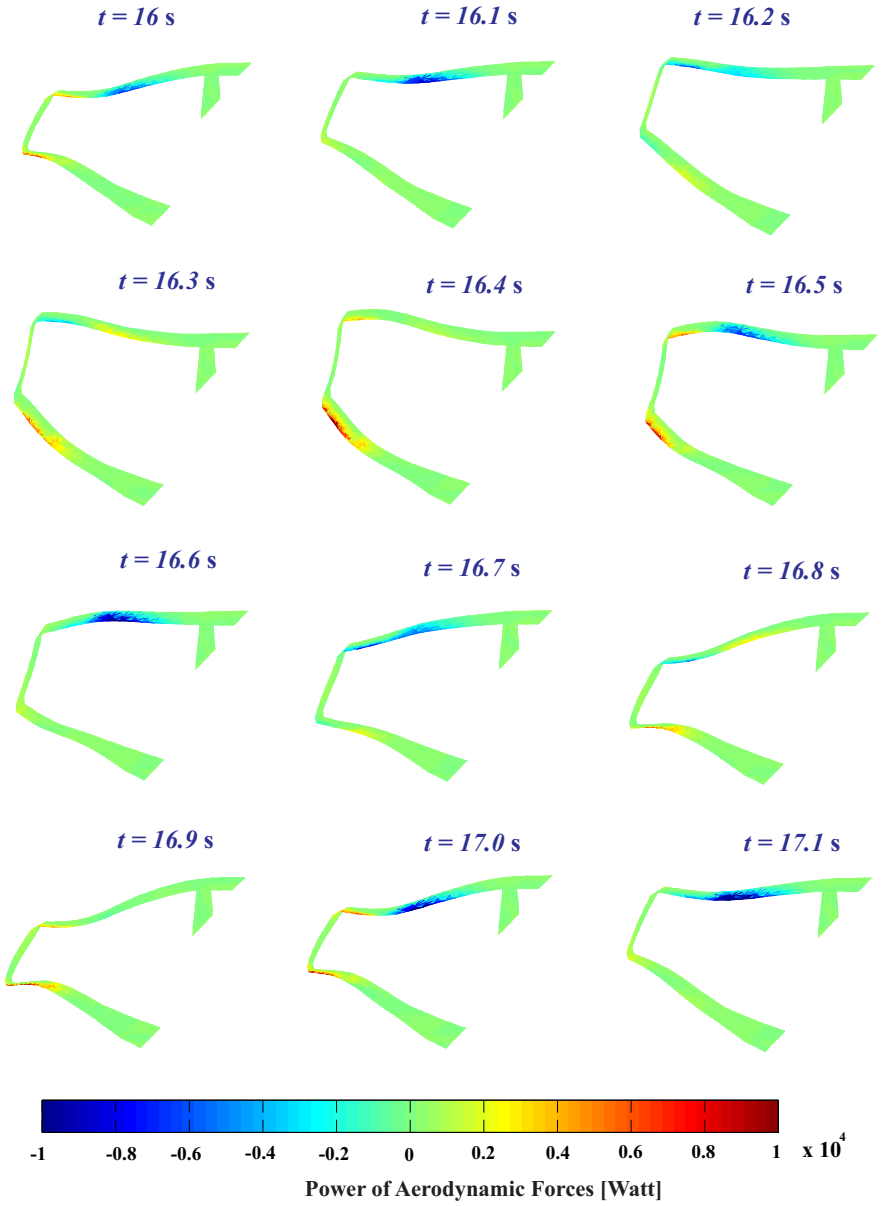

Fig. 14. Time response of the system for $V_\infty = 260$ m/s: magnified (5x) deformations and power of aerodynamic forces at different snapshots taken in the interval $16 \div 17.1$ s.

the *previous history*, and cutting it discards previous deformation patterns. Moreover, also for steady state cases, short wakes do not represent correctly the physical (and mathematical) problem and the interaction of the vorticity shed by a wing with the same wing or, in the present case, with other wings.

VI. Flutter of the PrandtlPlane with Freeplay

In this section, effects of freeplay of mobile surfaces will be studied. Freeplay is complicated to be precisely assessed and controlled in real situations. This is explained, for example in [56], where it is also stressed out how design can initially fulfill freeplay regulations, but, over aircraft's lifetime variations in parameters may lead to different aeroelastic response than the nominal one. This is shown in the paper as a strong sensitivity of LCO amplitude and frequency to freeplay angles.

Typically, freeplay is modeled considering a nonlinear rotational spring acting on the hinge line, and connecting the mobile surface to the wing. The response of such a spring in the *Moment-Angle* diagram, is

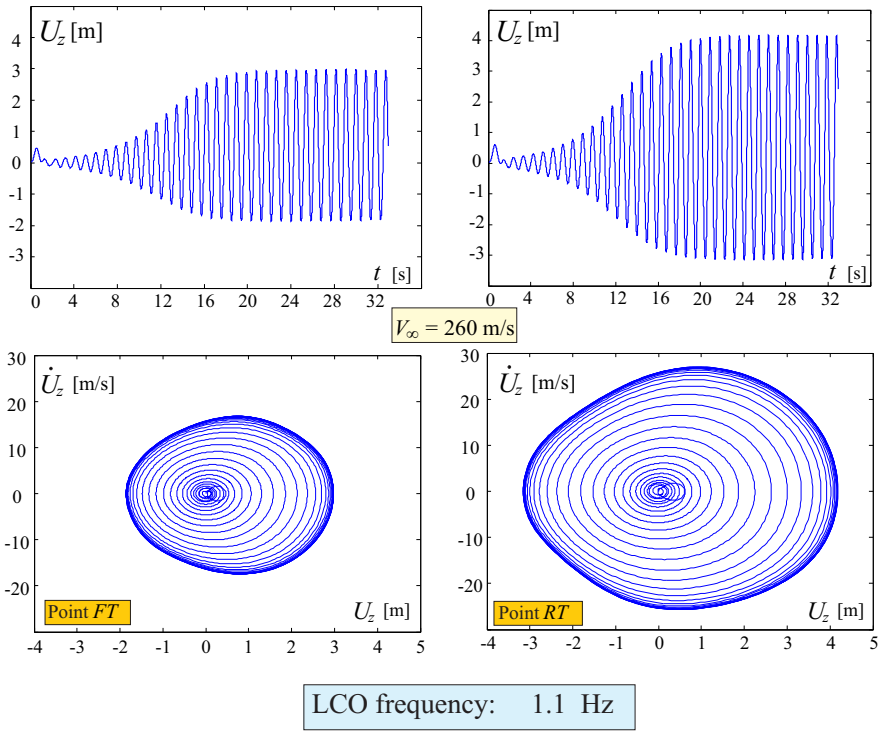

Fig. 15. Time response of the system for $V_\infty = 260$ m/s: vertical displacement of lower and upper wing's tips FT and RT, and phase-space diagrams.

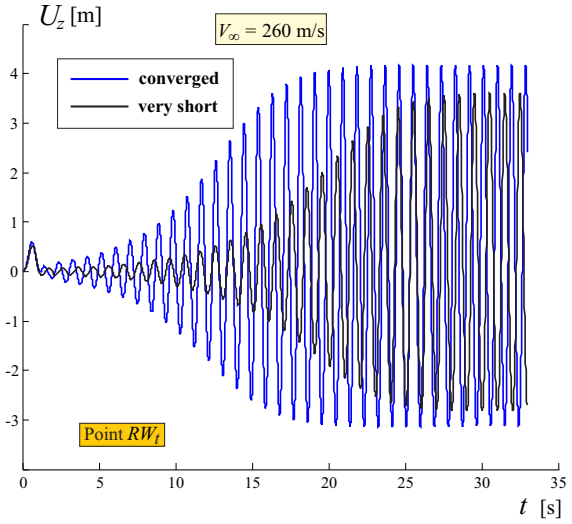

Fig. 16. Responses (vertical displacement of upper wing's tips RW_t) for different modeled wake's lengths.

usually described by a piecewise response: a linear dependence is chosen outside the freeplay interval, and a null response inside it. This model in inherently nonlinear. Slope outside the freeplay and interval of null reaction depend strongly on the actuation architecture.

When performing frequency-domain analyses about undeformed configurations, the angle is zero and thanks to the piecewise stiffness of the springs, the stiffness is zero (see Fig. 2). In other words, such a flutter analysis (*linearized stability analysis* of the aeroelastic system) is performed on a system in which locally the mobile surfaces can freely rotate.

In this section, different mobile surfaces are selectively and alternatively considered to have a freeplay.

When the flutter calculations are performed in the frequency domain the system is studied assuming it in the reference (undeformed) state. Thus, being the system linearized, the rotational stiffness of the springs is zero and the surface will be free to rotate. It will be observed that, in most cases, the same fundamental instability mechanism as when no freeplay is modeled, is still present at approximately the same speed. For some specific combinations of mobile surfaces having freeplay, the flutter speed could even increase.

Besides this main instability, *additional modes may become unstable* at relatively low speeds. These additional instabilities, however, persist for a limited range of speed values, and disappear when structural or other sources of damping are modeled. In some other cases, even after modeling the structural damping, a "persisting" instability associated to a higher mode and occurring at speed lower than the fundamental one is observed. To validate the frequency-domain analyses, the same approach of the previous section is pursued, i.e., both in-house and commercial tools are compared, and also a time-domain analysis is adopted to observe the response.

Effect of freeplay on LCO are also studied for a specific case. This exploits the full nonlinearity of the freeplay, showing how its amplitude is related to time-response of the system, in particular to LCO's amplitude and frequency.

Note that the present capability models both the *distributed* nonlinearity (structural geometric) and the *concentrated* one (piecewise description of the spring stiffness at the hinge of the control surface).

A. Freeplay of a single mobile surface

The goal of this work is to provide physical insights on the freeplay of the different surfaces. Thus, it is now investigated the case in which only a single surface (among all) presents the freeplay. All the other surfaces are considered "fixed".

1. *Front wing's elevator*

Freeplay is modeled for the front wing's elevator (see Fig. 6) only. Flutter analysis is given in Fig. 17 in terms of eigenvalues' real and imaginary parts. It can be inferred that the fundamental flutter mode (see the

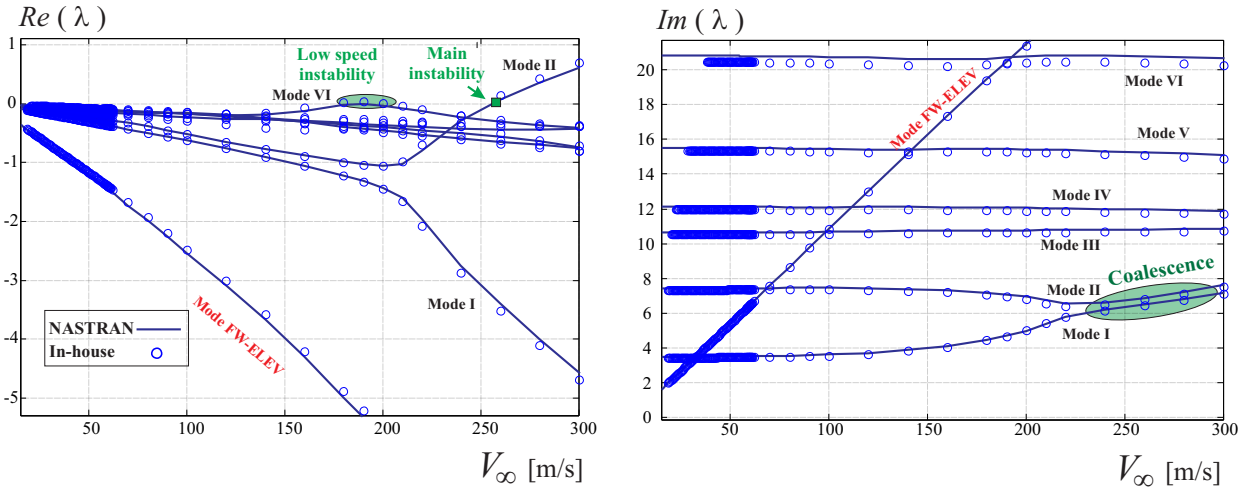

Fig. 17. Real and Imaginary parts of the eigenvalue of the system at different speeds. Free-play of the front wing (inboard) elevator (case *10000*).

"main" instability", mode II, in Figs. 10 and 17) becomes unstable at approximately the same speed as the case with no mobile surfaces. However, effects of the free elevator induce an instability of the sixth elastic mode, for which a flutter is observed at smaller speeds (see "Low speed instability", mode VI, in Fig. 17).

Before further proceeding it is important to stress out that this case has been verified with a convergence study by using refined aerodynamic meshes, refined structural grids and both simultaneously. Also the number of considered modes for the frequency-domain analysis has been increased and the effect on the results assessed. This approach was pursued for all the cases in which a relatively high-frequency mode was observed to become unstable.

The sixth mode is depicted in Fig. 18. Overall, the situation does not look very unfavourable. In fact,

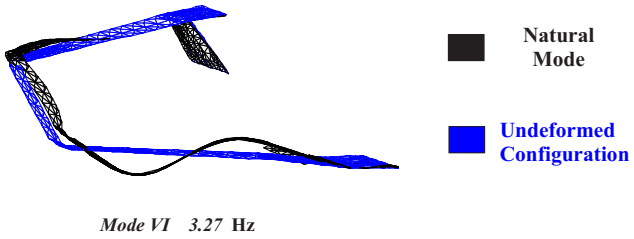

Fig. 18. Sixth elastic natural mode for the configuration with freeplay on the front elevator.

the "main" flutter speed (see the crossing of mode II in Fig. 17) has not dropped as it can actually happen in several situations (see the recent work on freeplay reported in reference [56]), and the instability of the sixth mode is limited to a very small range of speeds, suggesting that it can be easily "dominated".

Actually, the above analysis is on the conservative side since no structural damping was modeled. Considering a 1% damping ratio ($\zeta = 0.01$) changes the scenario to the one depicted in Fig. 19. It is evident how

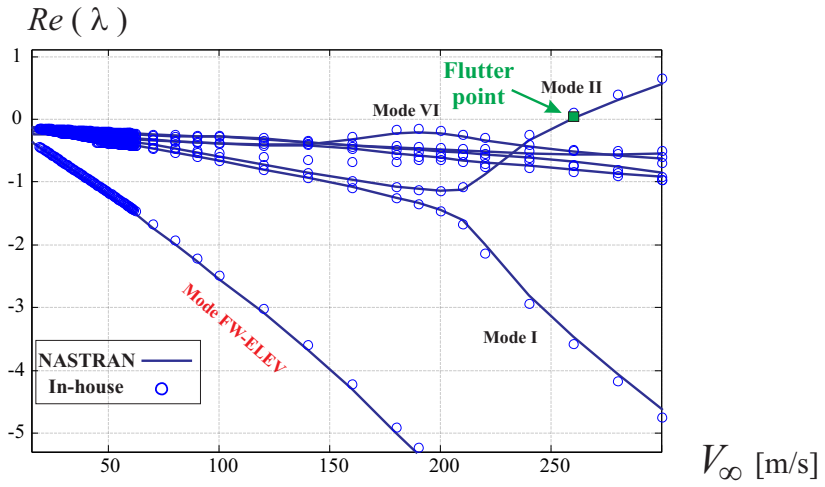

Fig. 19. Real parts of the eigenvalue of the system at different speeds. Free-play of the front wing (inboard) elevator (case *10000*), structural damping $\zeta = 0.01$.

the high frequency instability (mode VI, "Low speed instability" in Fig. 17) is eliminated: the sixth mode's real part of the eigenvalue no longer crosses the zero value for all the considered velocities.

2. Front wing's aileron

All control surfaces are now fixed except the front wing's aileron (configuration 01000). Flutter analysis is given in Fig. 20 in terms of eigenvalues' real and imaginary parts (structural damping is not considered). The scenario is similar to the previous case in which the front elevator was considered. Some high-frequency modes become unstable for a window of speeds in the low range. Again, considering a 1% of structural damping removes these instabilities, as shown in Fig. 21

An interesting point regarding this case is the increase in the "fundamental" flutter speed of about 10% when compared to the case without any freeplay, Fig. 10. In other words, having a freeplay on the front aileron posticipates the main flutter occurrence compared to the case without freeplay. This can be easily observed comparing Figs. 20 and 10. A time-domain analysis at the speed of $V_\infty = 260$ m/s supports the above finding. In fact, with reference to Figs. 22 and 12, the response to the same perturbation is strongly damped when the outboard aileron is left free. It is interesting to notice how the same mechanism of flutter, coalescence of the first and second frequencies is *posticipated* (see Fig. 23) when the front aileron is free to rotate. Thus, it may be inferred that the later occurrence of flutter is consequence of the interaction of the elastic modes with the rigid one concerning the aileron.

Trying to understand in depth flutter phenomena is always a formidable task. Dynamic response and

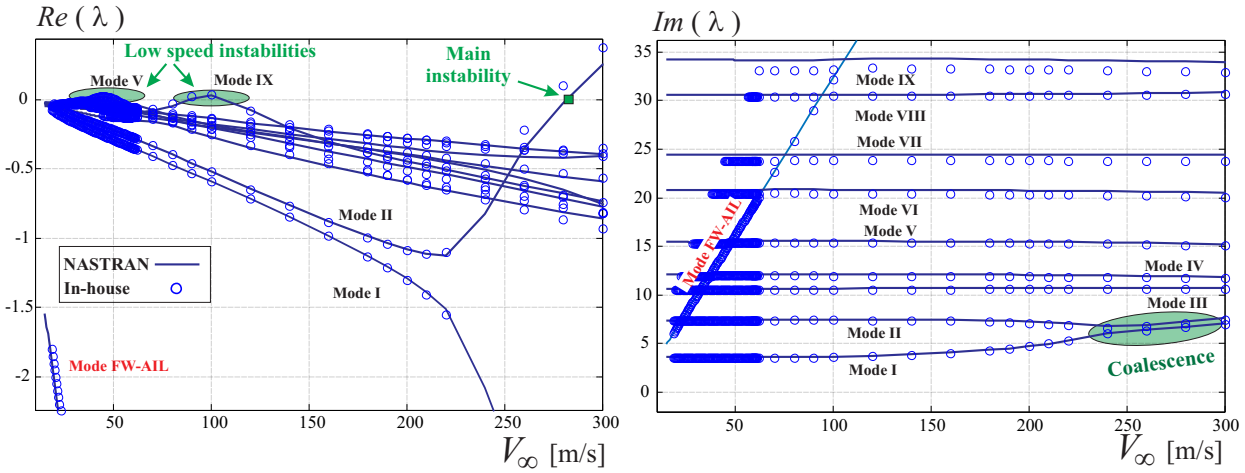

Fig. 20. Real and Imaginary parts of the eigenvalue of the system at different speeds. Free-play of the front wing (outboard) aileron (case *01000*).

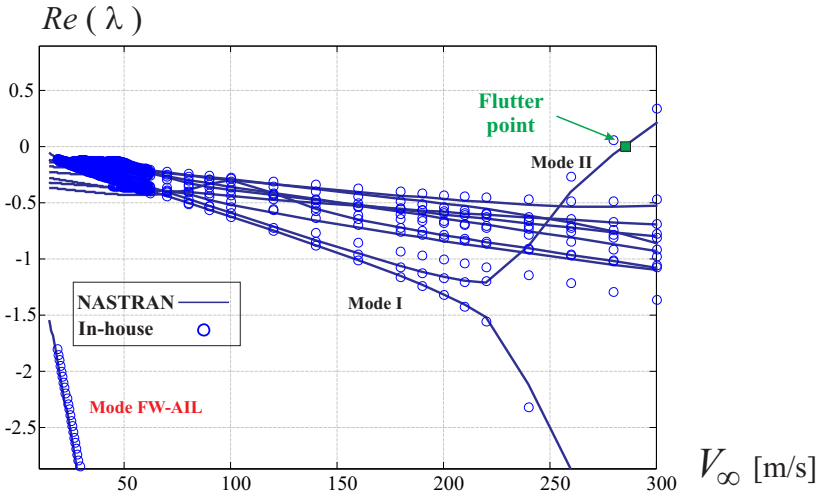

Fig. 21. Real parts of the eigenvalue of the system at different speeds. Free-play of the front wing (outboard) aileron (case *01000*), structural damping $\zeta = 0.01$.

energy exchange between the fluid and the structure can provide useful information regarding the flutter mechanism as will now be shown. With reference to the previous discussion presented in section V.A and Fig. 14, it was observed that lower wing was almost always extracting energy from the fluid. A more in depth inspection reveals that the tip region, in correspondence of the aileron, is where this exchange of energy is concentrated. It can be then speculated that, the presence of the aileron free to oscillate about the hinge line, interferes with this extraction mechanism, reducing it.

These findings can provide useful indications regarding passive *flutter suppression* methodologies specifically tailored for this airplane configuration. More in general, understanding the *energy transfer mechanism* between the structure and the flow provides valuable insight helping designing passive or active devices to suppress flutter.

This energy transfer may also suggest additional insights. In a previous study [16], different wake aerodynamic models were influencing by a large extent flutter speed of a box-wing layout. It was observed that different models were responsible of a load redistribution, especially in the tip region. In the light of the importance of the tip region for energy exchange, in particular, energy extraction from the fluid, it may be speculated that having a sensible mismatch on the aerodynamic forces in such a critical area can lead to consistent discrepancies in the flutter speed prediction. Obviously, this observation needs to be supported with more investigations to be conclusive.

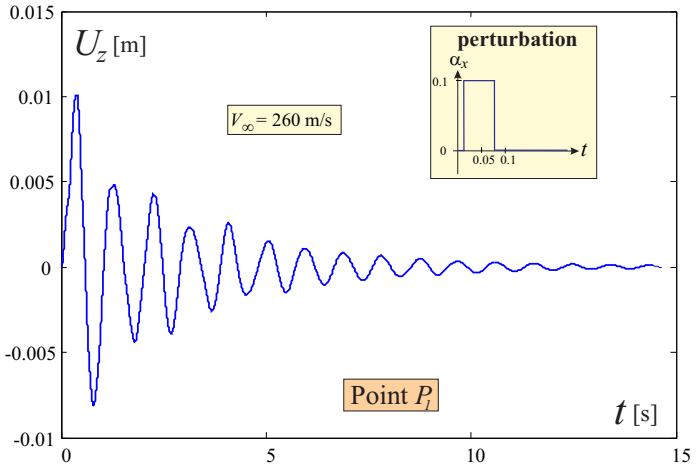

Fig. 22. Free front wing's (outboard) aileron. Time response of the system for $V_\infty = 260$ m/s: vertical displacement of the lower wing's tip (P_1).

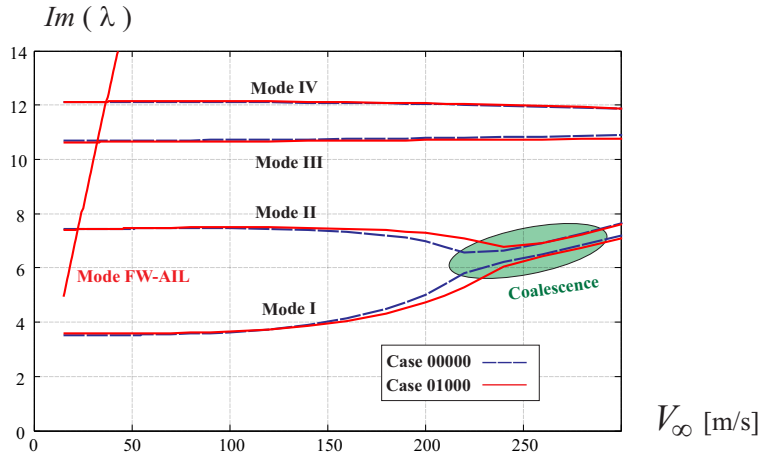

Fig. 23. Imaginary parts of the eigenvalue of the system at different speeds for the 00000 (all mobile mobile surfaces perfectly blocked) and 01000 (front aileron free).

Effects of aileron length The observed rise of the flutter speed is intuitively not expected since, as well known in literature (see for example Refs. [56, 57]), usually the aileron and elastic modes interact to anticipate the instability at lower speeds. With reference to one of the first studies in this regard, [57], the span width of the aileron in respect of the wing was varied and flutter characteristics were investigated. In effort [56] the aileron had larger span-extension when compared with the present one. This effect is here reproduced, modifying the span-wise length of the aileron, as shown in Fig. 24. Aeroelastic analysis on this configuration shows a dramatic drop in flutter speed when the aileron is free to rotate. See the real eigenvalue versus speed diagram in the same picture, and notice how the aileron's mode becomes unstable at relatively lower speed when compared to the shorter aileron version (case depicted in Fig. 21).

3. Rear wing's elevator

Considering the elevator on the rear wing free to oscillate (case 00010) leads to a completely different scenario than the one seen for the elevator on the front wing. Results of flutter analysis for this case are given in Fig. 25 in terms of eigenvalues' real and imaginary parts. Depending on the solver (in-house or NASTRAN), the 8th mode becomes unstable at a speed between $205 - 210$ m/s. This instability though, has different connotations than the previous observed non-fundamental ones. In fact, its instability persists and is not limited to a small windows of speeds. Moreover, the use of structural damping or nodal rotational dampers can't avoid its presence but, at most, postpone it to higher speed. Notice also that the same fundamental

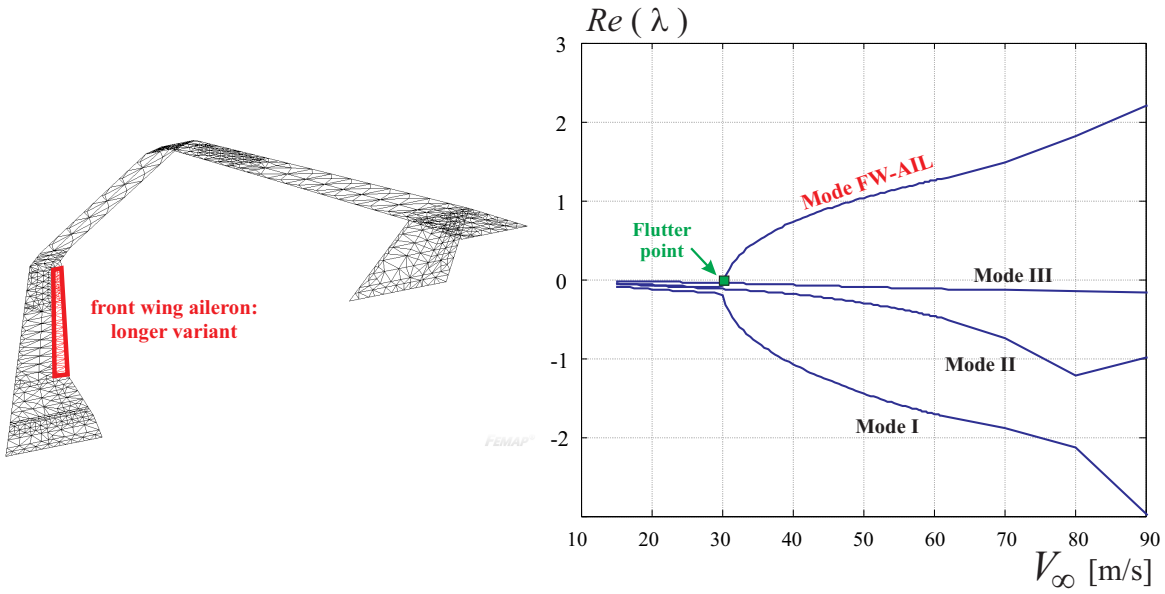

Fig. 24. Configuration with an enlarged front wing (outboard) aileron, used for demonstrating the drop in flutter speed. Real part of the eigenvalue of the aeroelastic system are plotted at different speeds.

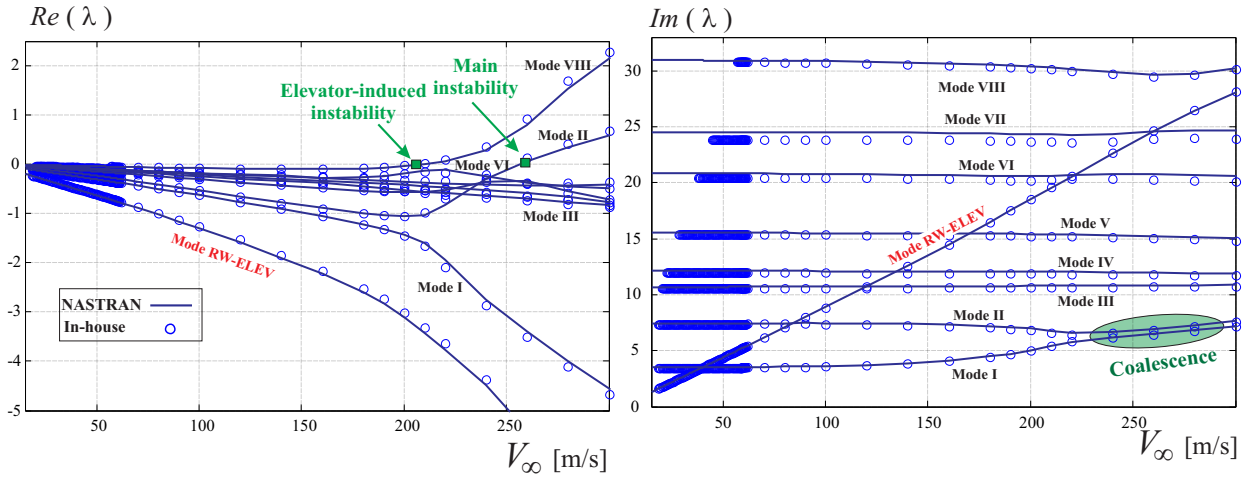

Fig. 25. Real and Imaginary parts of the eigenvalue of the system at different speeds. Freeplay of the rear wing (inboard) elevator (case *00010*).

instability with coalescence of the first and second mode still takes place.

As shown in Fig. 26 the 8th elastic mode mainly presents deformations of the aft wing: the bending of the wing is coupled with pitching induced by an in plane deformation of the vertical stabilizer. The front wing mainly presents in plane deformation.

A time domain response showing the dynamic instability is offered in Fig. 27, where vertical displacement of the points lying on the xz plane ($y = 0$), on the hinge line and trailing edge (HL and TE in the figure, respectively) of the elevator are depicted. This figure is obtained by performing the transient analysis for a speed larger than the flutter speed (post-flutter regime).

Fig. 28 shows snapshots (displacements are magnified by a factor of 5) at different times. Rear elevator area is responsible of energy transferring, and is where most of the displacements are located. However, also a front wing deformation can be appreciated.

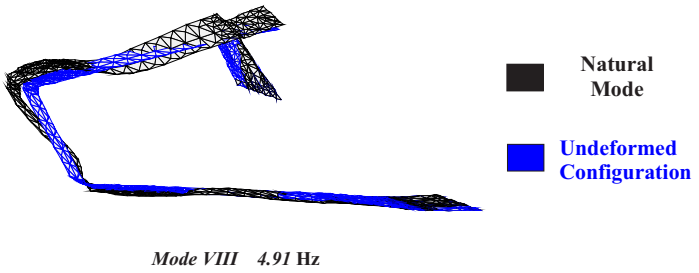

Fig. 26. Eighth elastic natural mode for the configuration with freeplay on the rear elevator.

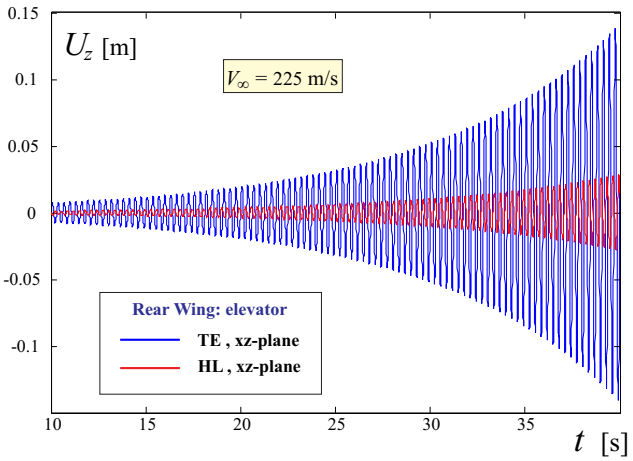

Fig. 27. Time domain response for the configuration with free rear elevator at a speed of $V = 225$ m/s.

4. Rear wing's aileron

Flutter analysis is given in Fig. 29 in terms of eigenvalues' real and imaginary parts. It is possible to notice that several modes (both lower and higher frequency ones) become unstable for a window of speeds in the low region. Moreover, the second mode looses stability at higher speed again ($V_\infty = 257$ m/s), and the fundamental flutter mechanism is then recovered. Structural damping ($\zeta = 0.03$) is considered in Fig. 30. Differently than the previous cases modeling structural damping does not eliminate the low speed flutter. Increasing the damping ratio may not be a conceptual sound approach, since damping modeling is per-se an art, and uncertainties in this regard need always to be considered.

Effects of dampers One option to eliminate the low speed instabilities is then to add dampers to the hinge line. This is, of course, a conceptual modeling approach, since in a real situation damping needs to be added to the complex actuator mechanism. Moreover, other means, like mass balancing, can be pursued. However, the aim of this study is to give an exploratory analysis showing that adding a "reasonable" source of damping will stabilize the system against low speed flutter.

As said, on the aileron hinge line rotational dampers are added. A value of specific damping of approximately 11.7 $\mathrm{N \cdot s \cdot rad^{-1}}$ is considered. This value is the result of applying 5 N·m/(rad/sec) concentrated dampers on each finite element node lying on the hinge line. Although in a real scenario it is unlikely this means to be used as damping source, it is interesting to notice that devices with such performances are available on the market. As shown in the frequency domain analysis, Fig. 30, using rotatory dampers eliminates the low speed instabilities.

A time-domain analysis is carried out at the speed of $V_\infty = 37$ m/s and $\zeta = 0.03$ with and without dampers, to show the different responses and confirm the frequency domain results. Results are summarized in Fig. 31.

It is worth to be noticed that this low speed instability induces very small deformations, which, in a real scenario may or may not produce appreciable effects. However, design needs always to comply with official

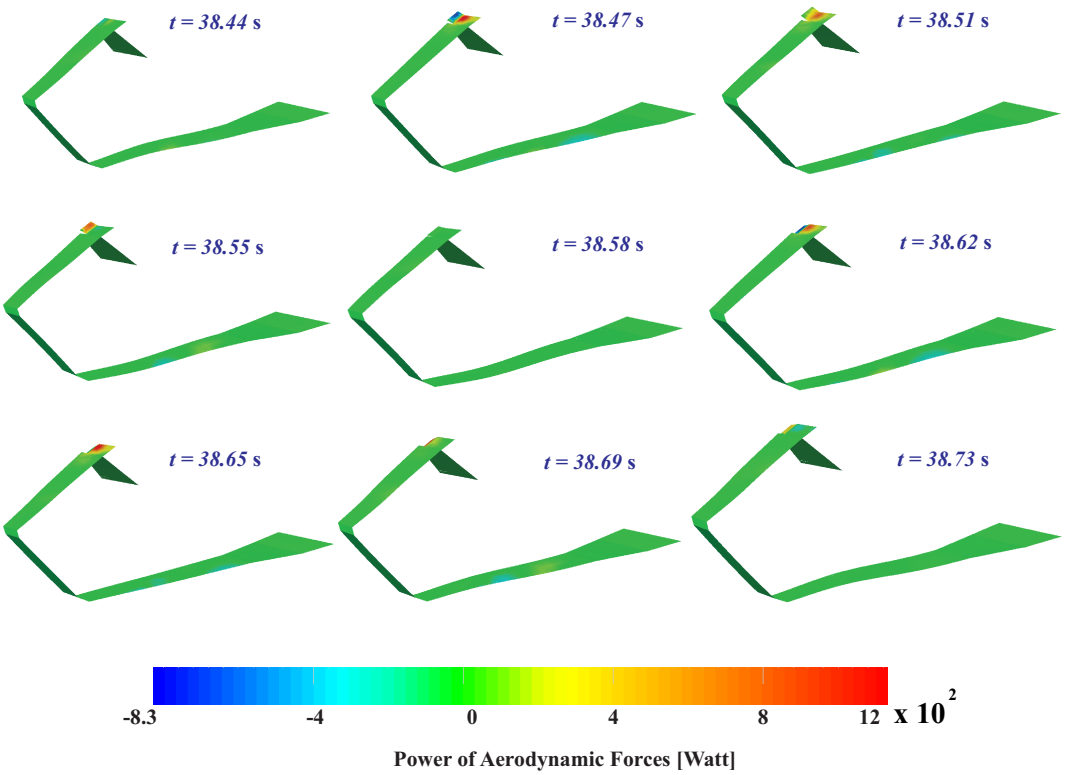

Fig. 28. Time response of the system with free rear elevator for $V_\infty = 225$ m/s: magnified (5x) deformations and power of aerodynamic forces at different snapshots taken in the interval $38.4 \div 38.7$ s.

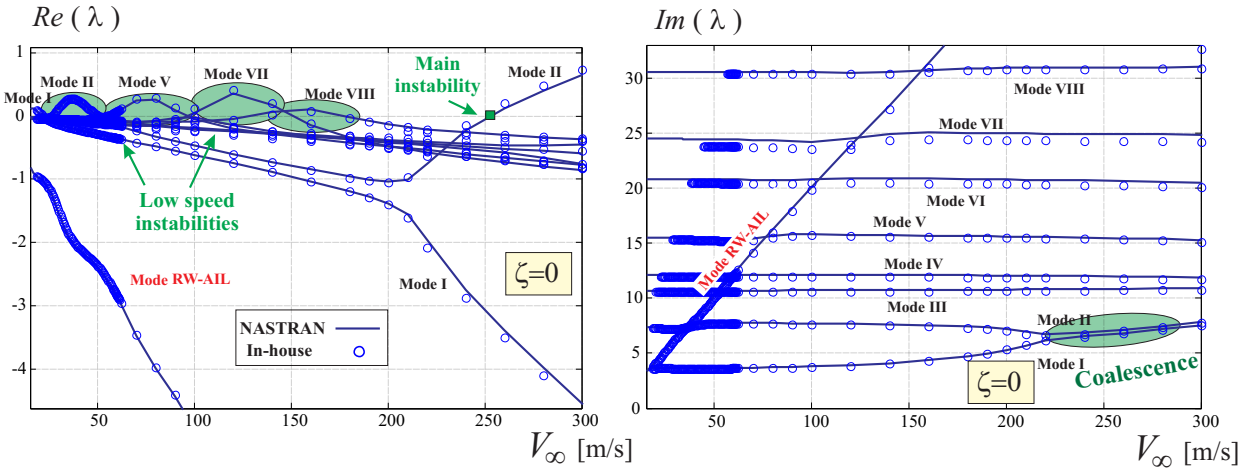

Fig. 29. Real and Imaginary parts of the eigenvalue of the system at different speeds. Free-play of the rear wing (outboard) aileron (case *00100*). The real part is plotted for different values of structural damping and dampers.

regulations.

B. Concurrent freeplay of two mobile surfaces

1. Rear wing's elevator and aileron

When freeplay is considered on both rear wing's elevator and aileron, the stability properties of the system are summarized in Fig. 32. Figs. 25 and 29, depicting stability properties when freeplay of the mobile

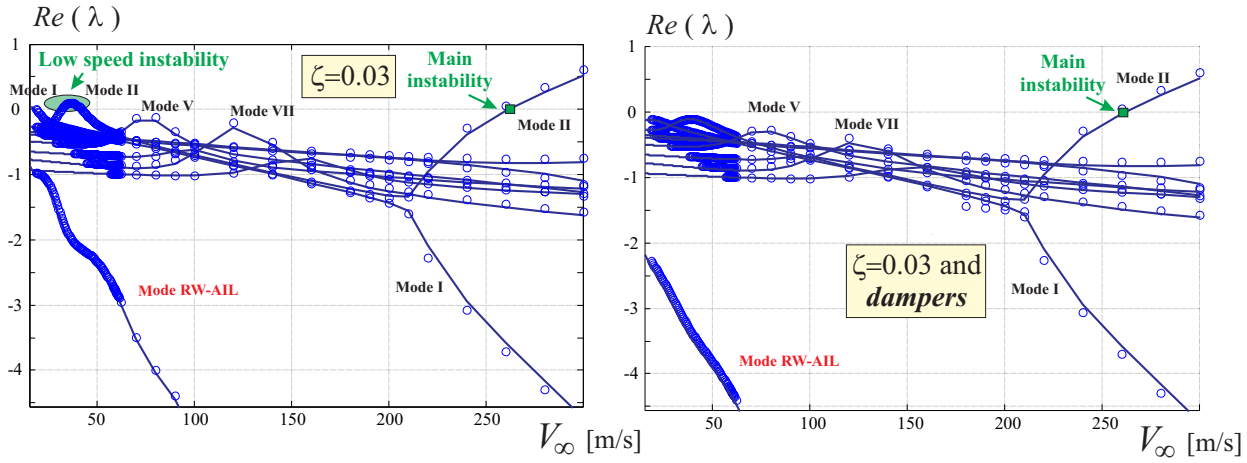

Fig. 30. Real parts of the eigenvalues of the system at different speeds. Free-play of the rear wing (outboard) aileron (case *00100*). Structural modal damping coefficient is $\zeta = 0.03$. On the diagram on the right, rotatory dampers are added along the hinge line.

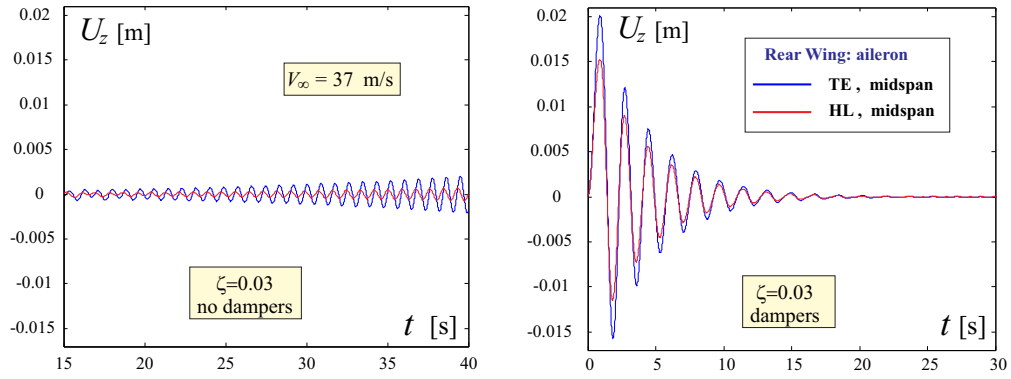

Fig. 31. Time response (after a perturbation is given) of the system with free rear aileron for $V_\infty = 37$ m/s: vertical displacement time history of the points on the hinge line (HL) and trailing edge (TE), at midspan aileron.

surfaces was selectively considered, help understanding the combined presence of freeplay. Instabilities in short windows of low speed are typical of the free rear wing outboard aileron case, whereas a "persistent" instability of the mode VIII was observed for the free elevator case. However, when the freeplay is modeled for the two mobile surfaces mode VIII becomes unstable at much lower speed.

In Fig. 33 the stability of the system (only real part of the eigenvalue) is depicted considering a structural damping, and eventually rotational dampers placed on the hinge line. A reasonable structural damping (damping ratio $\zeta = 0.03$) eliminates most of the low speed instabilities, moreover, it makes the fundamental instability (second mode) occur before the mode VIII's one. If rotational dampers are added on the hinge line of both the aileron and elevator (for the same amount of specific damping indicated above) then the low speed instabilities disappear. It is interesting to notice that 8th mode is not affected to an appreciable effect by the dampers.

C. Sensitiveness to freeplay amplitude

In the previous section effects of freeplay have been presented in terms of flutter analysis in the frequency domain. Thus, sensitivity to the interval of the freeplay (with reference to Fig. 2, the value of 2δ) and to the stiffness outside that interval (in the same figure, K_θ) were not investigated.

This section specifically considers the value of this interval and observes how the limit cycle oscillation (post-flutter regime) changes. In particular, the responses for $\delta = 0°$, $\delta = 1°$ and $\delta = 2°$ in the time domain are studied when freeplay of the rearwing's aileron is considered. The wind speed is $V_\infty = 260$ m/s.

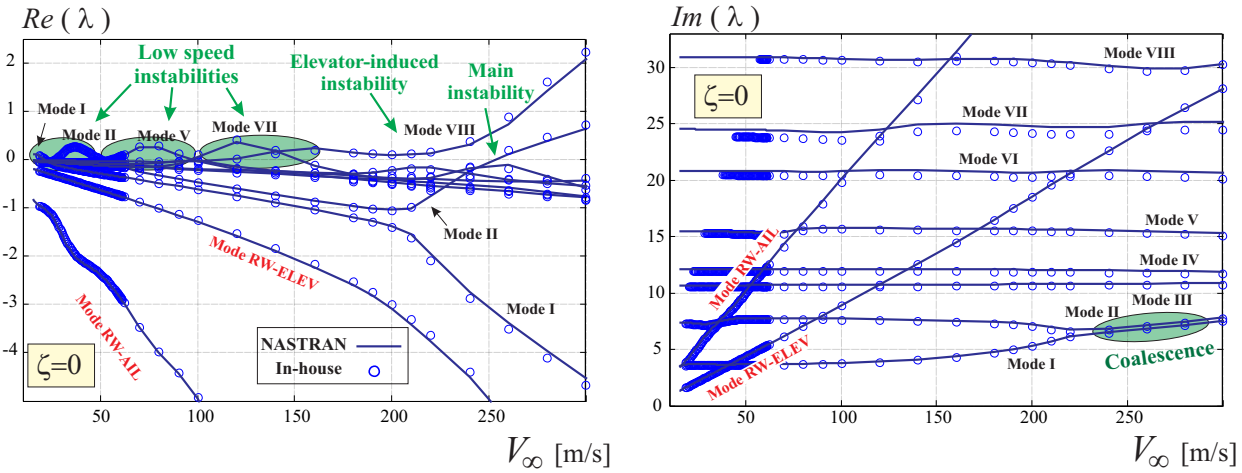

Fig. 32. Real and Imaginary parts of the eigenvalue of the system at different speeds. Free-play of the rear wing's elevator and aileron (case *00110*).

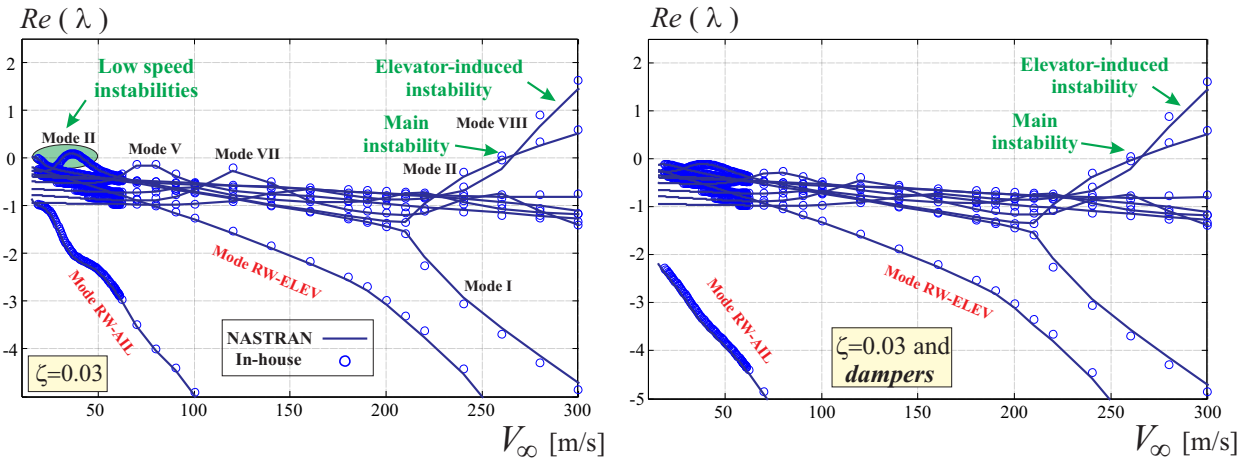

Fig. 33. Real and Imaginary parts of the eigenvalue of the system at different speeds. Free-play of the rear wing's elevator and aileron(case *00110*) when structural damping and dampers on the hinge line are modeled.

It is important to notice that regulations set the maximum allowable freeplay to *considerably smaller values* than those used here in the investigation. For example, according to effort [56], "the Joint Service Specification Guide (JSSG) prescribes for flutter a maximum allowable freeplay for an aileron located on the outboard wing section" of $\delta = 0.13°$. The larger values here employed are in an effort towards a conceptual understanding.

The model implemented for correctly taking into consideration freeplay law was described in section III.A.1. Results of the investigations show that effect of freeplay on LCO amplitude are quite negligible. As it could be inferred from Fig. 34, depicting the time response (vertical displacement of the lower wing's tip) to a disturbance in angle of attack, the LCO amplitude in the cases $\delta = 1°$ and $\delta = 2°$ does change to a very small extent, in the order of 3%. Actually, interestingly, when freeplay is larger LCO is smaller.

Work [56] considered a cantilever wing, with a mobile surface extending through a large portion of the wingspan. Due also to larger mobile surface relative span, aeroelastic dynamic properties were completely different when freeplay was considered (as compared to the $\delta = 0°$ case). Moreover, LCO amplitude was very sensitive to freeplay: wider patterns were observed as consequence of larger δ.

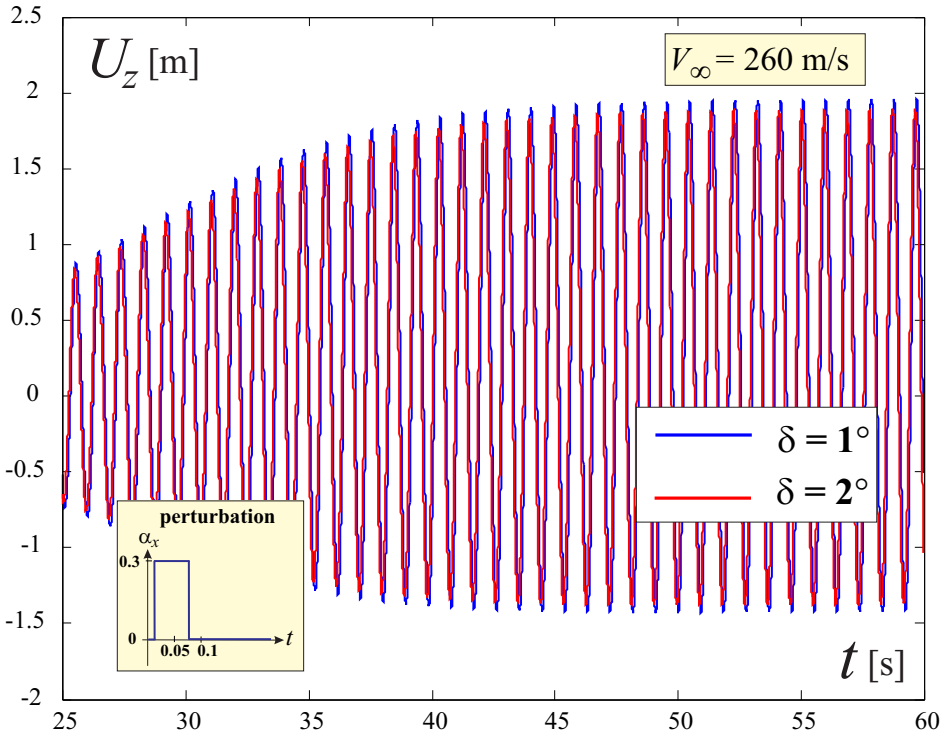

Fig. 34. Effects of freeplay δ on the amplitude of the LCO: vertical displacement of lower wing's tip in time.

VII. Body-freedom Flutter Analysis of the Baseline Configuration

In this section flutter analyses on baseline configuration are carried out considering also the (symmetric) rigid body modes. Differently than a real trimmed aeroelastic investigation, the flutter is evaluated about the undeformed configuration. Since no geometrical twist inducing any geometrical angle of attack is included in the aerodynamic description, the undeformed configuration carries no lift when asymptotic angle of attack is zero, i.e., the undisturbed flow is parallel to x-axis.

A further issue to take into account is the static stability (on a flight mechanics perspective), which was guaranteed by the preliminary design of the layout carried out in Refs. [18,20]. Since the here used equivalent model relies on the same aerodynamic surface and the difference in the position of the center of gravity is negligible, the margin of stability remains approximately the same.

Historically, the most notable cases of interaction between rigid body and elastic modes in aeroelastic applications go back until the pre World War II, on Flying Wings-like configurations (see work [58] for an interesting historical background). Such an interaction was named *Body Freedom Flutter* (BFF). Example of early experimental investigations involving BFF are [59, 60].

For Joined Wings, low frequencies of the first elastic modes have been observed in different cases (see effort [36] for a Box Wing case, [61] for "Diamond Wing"). For this reason, Joined Wings have been considered potentially prone to interaction between the elastic and rigid body modes [37, 62], changing the flutter properties from the idealized fixed (cantilever) case. Notice, that these low frequency values do not guarantee, per se, the above prospected interaction, playing the relative fuselage/wing mass and inertia, and also the configuration flight mechanics properties a relevant role [59]. This section aims to characterize the *Prandtlplane* behavior in this regard.

A. Modeling approach

In order to take into account the rigid-body modes of the aircraft, the fuselage effects have to be modeled. If it is true that an acceptable inertia and stiffness distributions are needed in order to give conclusive results, it is also true that fuselage models for this configuration are very complicated (see for example Ref. [63]) to be described with the similar level of fidelity characterizing the wings. Thus, as a first preliminary step,

the fuselage has been considered as completely rigid. Moreover, its inertial properties are extrapolated considering the real position of the center of gravity of the whole configuration (see Refs. [20, 35, 64]), deducing the fuselage overall weight (comprehensive of payload) and evaluating its moment of inertia with arguments based on similarity. It holds that nominal fuselage mass is $M_{\text{fus}}^{\text{ref}} = 9.1 \cdot 10^4$ Kg, and (pitching) moment of inertia $I_{\text{fus}}^{\text{ref}} = 1.2 \cdot 10^7$ Kg·m^2. The fuselage inertial properties may change to a large extent the response of the system. For this reason, investigations carried out with the above reference values may be of limited value if not augmented with a sensitivity analysis, as pursued in the following sections.

To model the above target inertia properties, concentrated masses have been appropriately placed on the front wing- and fin-fuselage connections. To avoid local unrealistic in-plane deformations, these sections have been reinforced connecting the nodes with rigid links. See Fig. 35 for a conceptual representation. The same elements were used to rigidly connect the front wing and fin, guaranteeing rigid body motions of the aircraft. The connections represented in the same picture do not represent the real arrangement, which was pursued carefully avoiding relative rigid motions between some nodes.

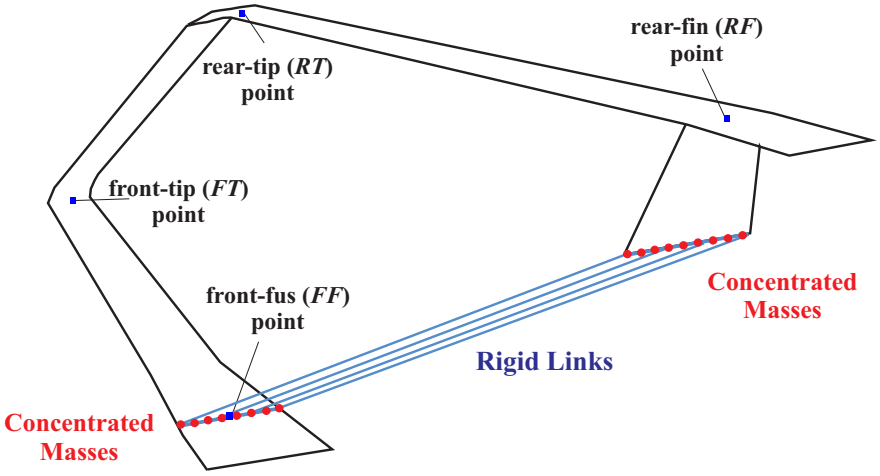

Fig. 35. "Free-flying" conceptual model. Notice the concentrated masses and the rigid links.

The above modeling is consistent with the objective of conducing symmetric "free-flying" analyses, where with symmetric is intended that only plunging and pitching motions are considered. A full "free-flying" analysis should also consider the antisymmetric modes (and evaluate the elastic modes on the deformed trimmed configuration), and in this case the above placements of the concentrated masses has to be revisited since it does not describe the proper inertial moment in the latero-directional plane.

To specifically assess the value of concentrated nodal masses (modeling inertial effects of the fuselage), an algorithm was written able to comply with these three constraints:

a) fuselage's target mass;

b) fuselage's target moment of inertia;

c) position of the of center of gravity projection on the symmetry plane.

B. Preliminary results on a front-wing-only layout

To assess the capability of such modeling procedure to capture body-freedom flutter, the configuration composed of the front-wing and a lighter version of fuselage is first considered. Analyses carried out with NASTRAN are shown in Fig. 36, where only the two rigid body modes and the first three elastic ones are depicted. As clearly shown, the rigid modes do not *significantly* interact with the elastic ones.

However, when the fuselage is not modeled (or, equivalently, it has a negligible mass and inertia), there is an interaction between the first (elastic) mode and the pitching (rigid) mode, see Fig. 37. This same strong interaction between rigid and (first) elastic (bending) mode was the one usually observed for flying wings, for which the notion of BFF was introduced. Obviously this example has been carried out only with the purpose of validating a model and procedure, and does not carry any quantitative information (the configuration might even be unstable from a flight mechanics point of view).

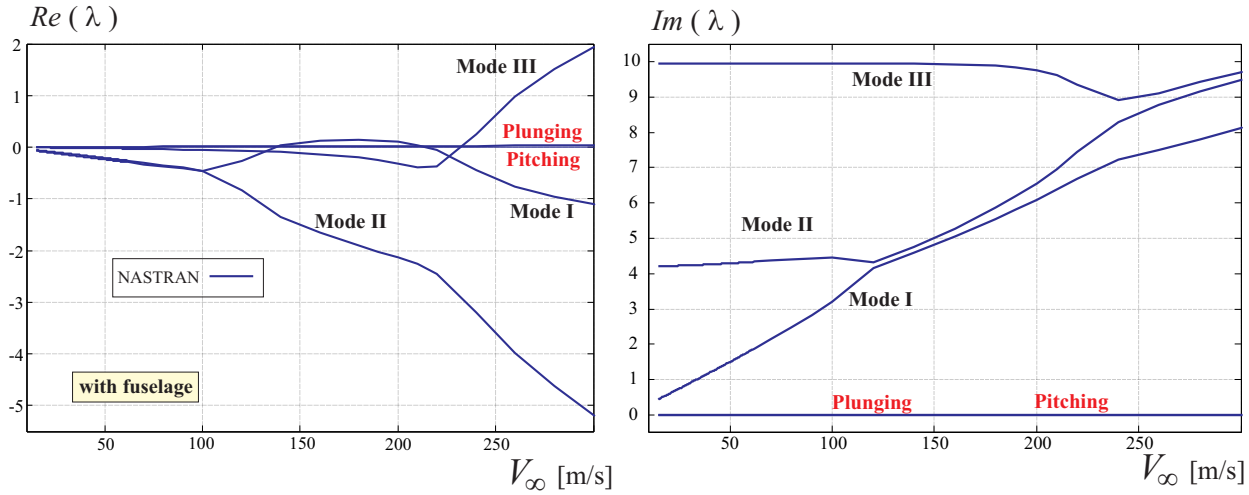

Fig. 36. Real and Imaginary parts of the eigenvalue of the front wing plus scaled fuselage system, at different speeds.

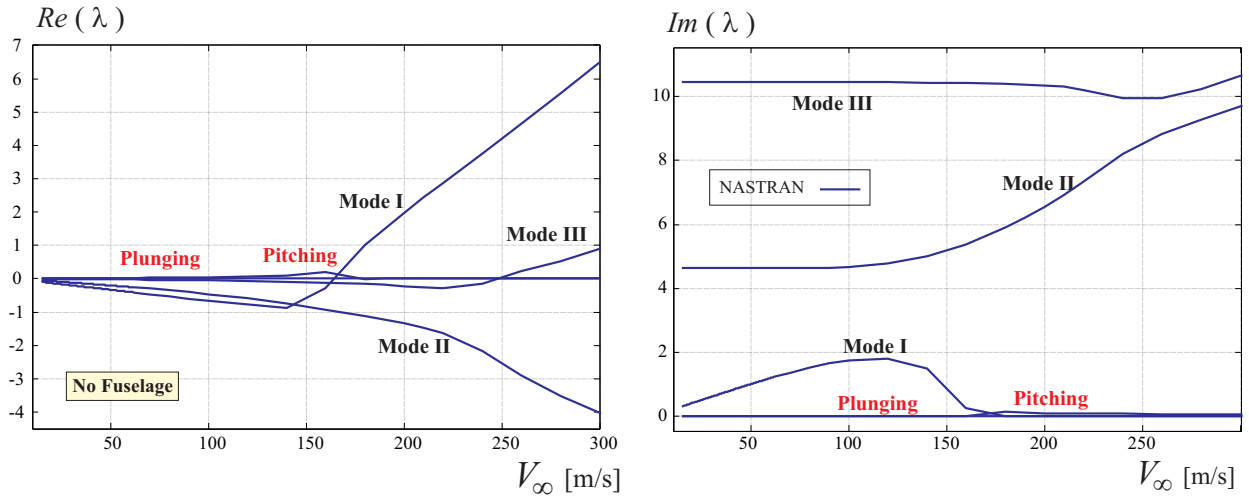

Fig. 37. Real and Imaginary parts of the eigenvalue of the front wing without fuselage system, at different speeds.

C. Results for the PrandtlPlane

The natural modes of the system are first depicted in Fig. 38. Results of the flutter analysis with the in-house code and NASTRAN present an excellent correlation, see Fig. 39. The flutter occurrence is not represented because the analyses were carried out for incompressible cases ($M = 0$), whereas, as far as speed is increased the approximation of neglecting compressibility effects is progressively less justified (even at sea level).

The fact that a "free-flying" analysis would not, according to the frequency-domain analyses, experience flutter within the considered speed domain, whereas the constrained model is (compare Figs. 10 and 39), poses some questions that need to be addressed. First, it should be again remarked that a thorough analysis needs also to consider the real fuselage design, the aircraft (aeroelastically) trimmed at different flight conditions within the flight envelope. However, the present effort represents a first step in this direction and may give some important preliminary indications. The question is then, how sensitive are the aeroelastic stability properties of the system to inertial parameters? How do they change with fuselage mass and pitching moment of inertia?

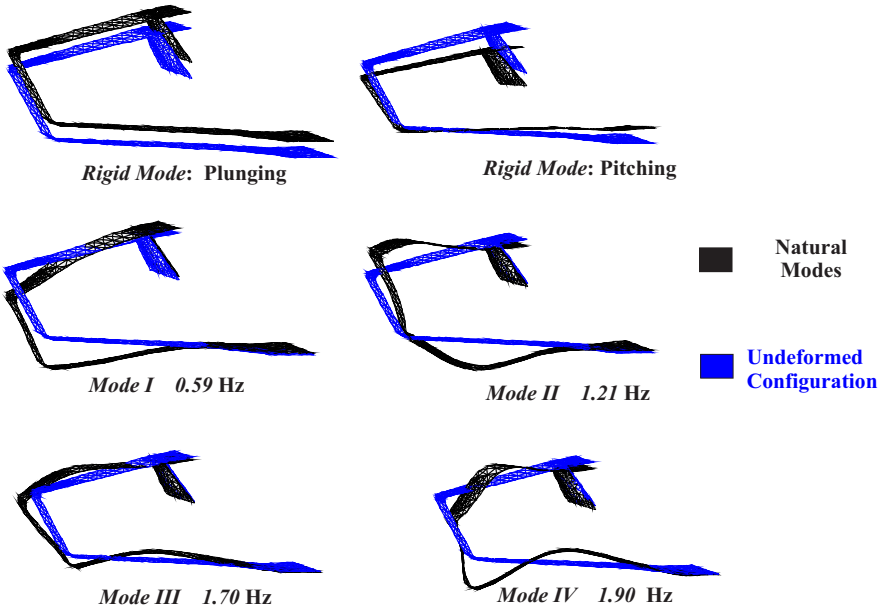

Fig. 38. Two rigid modes (plunging and pitching) and first four elastic modes with associated frequencies.

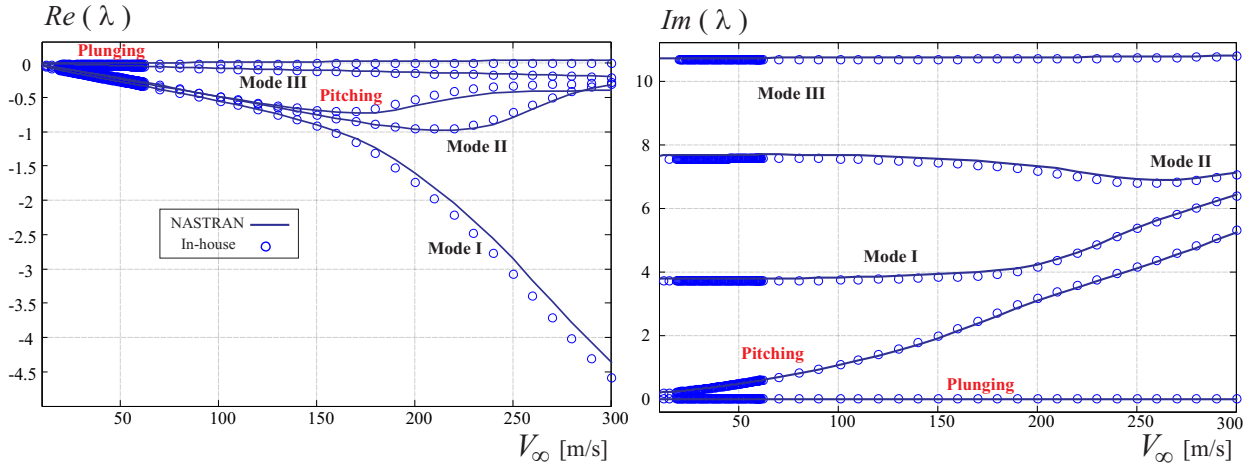

Fig. 39. Real and Imaginary parts of the eigenvalue of the PrandtlPlane plus fuselage system, at different speeds.

1. *Time response*

A time-domain analysis of the response of the "free-flying" model to a vanishing perturbation is here presented. This is carried out both for low and high speeds.

It is important to remark that these analyses are intended to help interpreting results obtained with the frequency domain analyses, and not as independent real trimmed aeroelastic analyses. In fact, the initial (linearization) configuration is undeformed, the angle of attack is zero, and null are also the lifting forces.

The here-used time-domain aeroelastic solver employs vortex-rings, the interface algorithms rely on a moving least squares (MLS) approach, as described in Refs. [16,17]. The rings are located on the undeformed surface, and they do not follow the structure in its displacement. Conversely, the deformation is taken into account updating the normal used both in the tangency-wall condition and in the Kutta-Joukowsky force formula.

LOWER SPEED CASE The air speed is set to $V_\infty = 50$ m/s. A vanishing perturbation in angle of attack α_{flow} is given, as depicted in the box of Fig. 40. This particular symmetric shape is adopted in an effort of avoiding

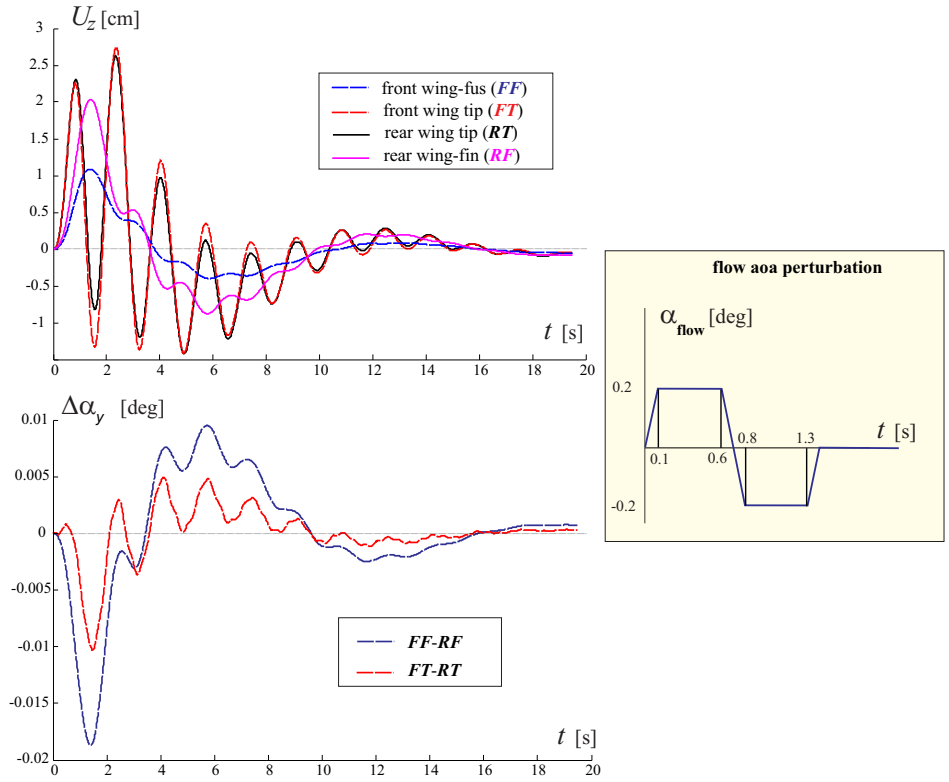

Fig. 40. Time response for $V_\infty = 50$ m/s. The perturbation in flow angle of attack is depicted in the box. Above, vertical displacement of the four points on the mid-chord (front and rear wing's tips - FT and RT, front wing-fuselage and rear wing-fin connection - FF and RF) are depicted. Below, the geometrical rigid rotations of the fuselage/fin (FF-RF) and tip/tip (FT-RT) segments along axis-y are given.

a strong tendency to depart too much from the planes where aerodynamic singularities are positioned. Due to the adopted load-displacement interface (where singularities maintain their position regardles of wing's deformation), this guarantees an acceptable precision.

Time-response of the different test points is also shown. The test points are all lying on the mid-chord of different span locations, and on different wings. Point FF lies on the front wing, at the hypothetical intersection with the fuselage, FT and RT are on the wing's tip, whereas RF lies on the connection between the rear wing and the fin (see Fig. 35 for a pictorial representation of the points). On the same figure, below, it is depicted the evolution of values of two angles. The first one is the variation of the angle (measured in the plane XZ) of the segment connecting the points FF-RF and FT-RT. Since the point on the fuselage and the one on the fin's root are rigidly connected, it can be assessed as the geometrical angle of attack of the aircraft.

As it can be inferred from Fig. 40, after a transient the displacements settle to zero. This means that the elastic deformations and also the rigid body motion slowly vanish.

HIGHER SPEED CASE A larger speed is here considered, namely $V_\infty = 260$ m/s. The same vanishing perturbation is here adopted (although the peeks are smaller, namely $0.01°$). This case is interesting because it can be compared directly to investigation carried out at the same speed for cantilever aircraft, see Fig. 12 and section V.A, showing an unstable behaviour.

Fig. 41 depicts the response. From an aeroelastic point of view, the oscillations vanish, whereas at the same speed the cantilever model was unstable. A very small (notice the scale in Fig. 41) rigid vertical translation is noticed. Current investigations are aiming to understanding this point, and assess if it is an artifact of numerics or is related to the plunging mode.

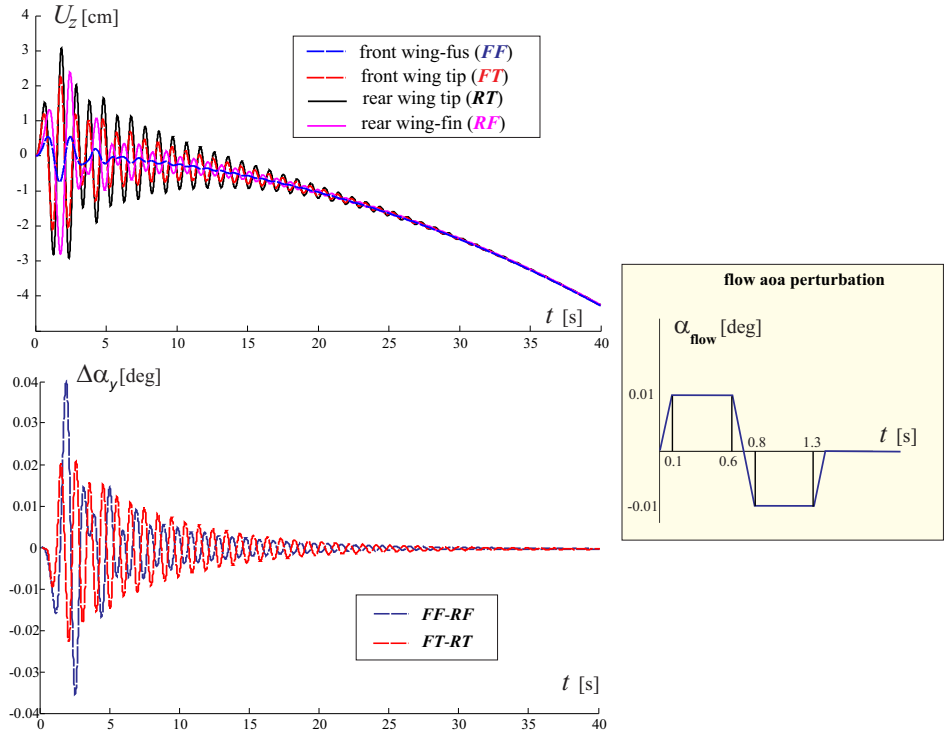

Fig. 41. Time response for $V_\infty = 260$ m/s. The perturbation in flow angle of attack is depicted in the box. Above, vertical displacement of the four points on the mid-chord (front and rear wing's tips - FT and RT, front wing-fuselage and rear wing-fin connection - FF and RF) are depicted. Below, the geometrical rigid rotations of the fuselage/fin (FF-RF) and tip/tip (FT-RT) segments along axis-y are given.

2. *Sensitivity to fuselage's mass and moment of inertia*

As stated, effects of uncertainties in the determination of the fuselage moment of inertia need to be carefully assessed. For this reason, some sensitivity analyses are here presented, in which the mass of the fuselage and/or its moment of inertia are changed. However, the same position of the center of gravity is maintained to keep the same margin of stability.

Fuselage Mass variation If the *mass of the fuselage is increased, the flutter speed drops.* In particular, when its value is increased of an 80% of the original weight, flutter is observed for a speed of $V_\infty = 253$ m/s. However, this drop in instability onset speed should carefully be understood. In fact, it does not represent the limit toward the clamped case. This can better argued with aid of Fig. 42, showing the stability properties of the system when two heavier fuselages are considered. Comparing the diagram with the one of the cantilever system, Fig. 10, now the the pitching mode is the one turning unstable (and not the second one). Mode II, on the contrary, is stable. Coalescence of the pitching and first elastic mode is noticed, whereas the classic coalescence characterizing the fundamental flutter of the fixed configuration, involving first and second elastic modes, seem to be posticipated.

Fuselage Moment of Inertia Variation Now, the mass of the fuselage is kept constant to its nominal value, whereas the inertia is increased. With reference with Fig. 43, it can be inferred that second mode becomes critical at lower speeds when the moment of inertia increases. As expected, the frequency domain suggests that now interaction of the pitching mode with the elastic ones is weaker, and coalescence of the mode I and II is anticipated. This picture shows how, *in the limit of increasing pitch inertia, the cantilever system stability properties are recovered.*

Discussion Results above can be reinterpreted to show how there is a passage from BFF to cantilever flutter type when the fuselage pitch inertia- increases (for a fixed weight). With cantilever flutter it is intended the flutter occurring when mode II becomes unstable and a coalescence between frequencies modes I and II is observed: this is exactly the mechanism observed in the previous sections for the cantilever system.

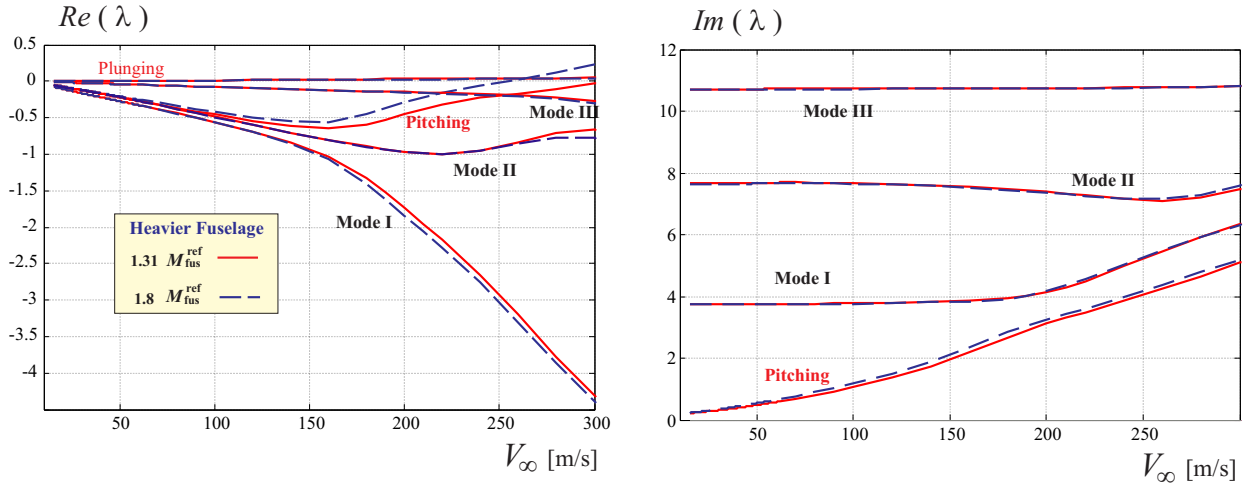

Fig. 42. Real and Imaginary parts of the eigenvalue of the PrandtlPlane with heavier fuselages (moment of inertia of the fuselage and location of system's center of gravity are kept to the reference values).

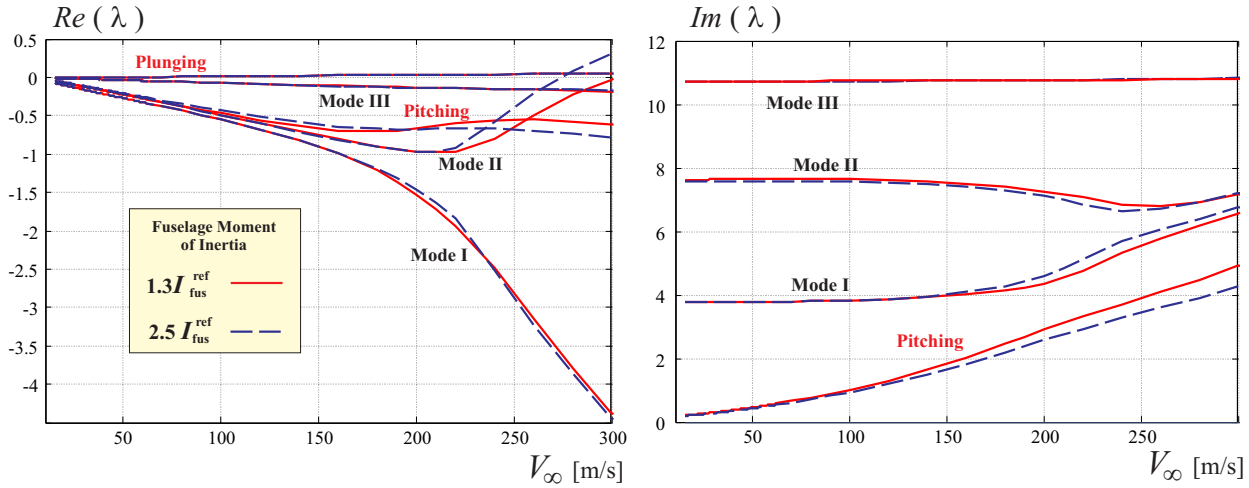

Fig. 43. Real and Imaginary parts of the eigenvalue of the PrandtlPlane with fuselages with larger moment of inertia (fuselage weight and location of system's center of gravity are kept to the reference values).

The pitching inertia is varied from $0.1 \cdot I_{\text{fus}}^{\text{ref}}$ to $4.3 \cdot I_{\text{fus}}^{\text{ref}}$. With reference to Fig. 44, in the lower pitching inertia case (dashed lines), the flutter is of the BFF type, involving pitching mode (depicted in green). On the contrary, mode II (in red) is well in the stable region. There is also a coalescence of the pithing and first elastic mode.

In the nominal case (thin continuous lines), within the speed range, all the modes are stable. Thus, no flutter is observed for this case. For mode II (in red), the margin of stability (here intended as the distance of the real part of the associated eigenvalue from 0) decreases. Frequencies of pitching (green) and first (blue) modes do not get as close as before. The opposite trend is observed for the frequencies of mode I and II. This is the prelude to a change in the stability properties.

When pitching inertia is further increased (dotted-dashed lines), flutter is observed, associated with the same properties of the cantilever system case: mode II (red) becomes unstable. Coalescence of modes I and II is observed in the frequency-speed diagram, whereas pitching mode frequencies keep far from the ones of the first mode.

Summarizing, for a fixed mass, for lower pitching inertia the aeroelastic stability properties is characterized by BFF, whereas, for large values, cantilever flutter is observed. For some values of the moment of inertia between the above limiting cases (like the nominal chosen one) flutter won't be observed within the speeds of interest.

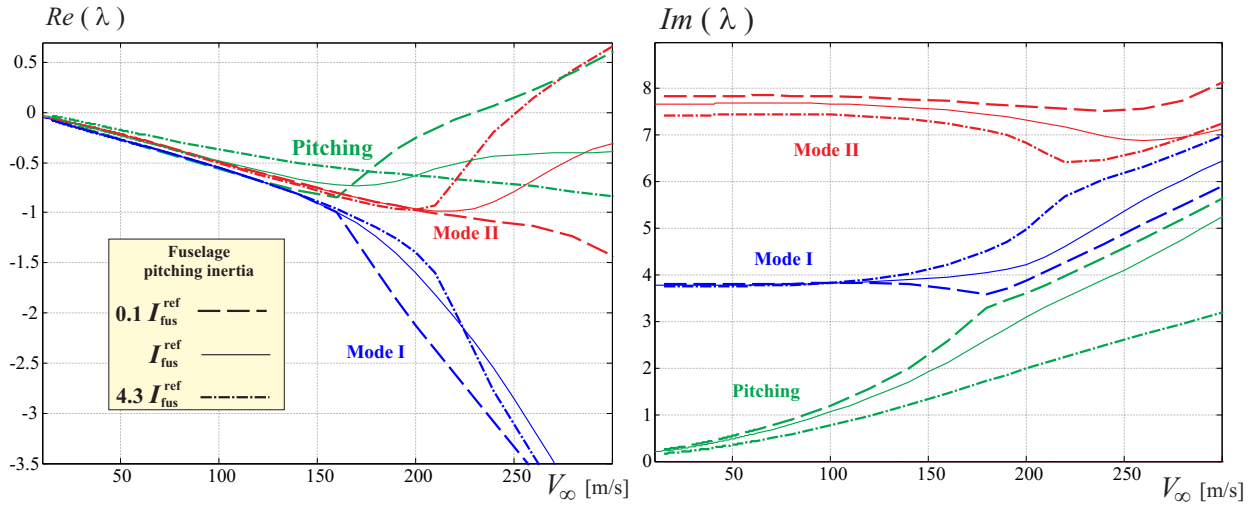

Fig. 44. Real and Imaginary parts of the eigenvalue of the PrandtlPlane when pitching inertia is varied (location of system's center of gravity is kept fixed).

As stated in different literature efforts [37,58,62], BFF can also be favoured by a relative small separation between the elastic modes and short-period frequency. Short period frequency increases when pitching moment decreases, reducing thus the gap from the elastic modes frequencies (which for Joined Wings are inherently small) and promoting the interaction.

VIII. Conclusions

This effort has contributed to shed light on the dynamic aeroelastic behaviour of a joined-wing configuration called *PrandtlPlane*. The *first* contribution was the study of the flutter phenomenon also from a post-critical perspective. A limit cycle oscillation was observed, and its pattern, strongly involving tilting of the joint, depicted. Time domain response was very useful to study the power transferred from the fluid to the structure. It was highlighted that, the front wing had a destabilizing aeroelastic effect since it extracts energy from the fluid. The most active region in this energy exchange was the tip.

In the framework of Joined Wings and for the first time, this work also studied effects of freeplay of mobile surfaces on aeroelastic properties. It was found that in some cases, a few modes were unstable for a small range of speeds in the low spectrum, however, the same "fundamental" flutter mechanisms was observed at high speed. Adding a structural source of damping (structural damping or rotational concentrated dampers on the hinge line) was showing to eliminate the low speed issues.

Freeplay on some specific mobile surface (front wing's aileron) was found to have impact also in this "fundamental" instability. In particular, flutter speed was observed to be consistently increased. With reference to the energy diagram, this phenomenon was attributed to a "disturbance" of energy-transfer mechanism in an area mainly extracting energy from the fluid.

In some other cases, freeplay was inducing an higher-mode instability, occurring before the "fundamental" flutter. Contrary with the previous situations, the instability was persisting and not confined to a small window of speeds. Thus, addition of damping and dampers had the effect of only slightly posticipating its occurrence, but not eliminating it.

The *third* contribution concerned the flutter analysis when rigid body modes were considered, i.e., a free-flying flutter analysis. For the baseline configuration, the interaction between the rigid and elastic modes proved to be beneficial, since no instability was occurring within the range of considered speeds. For having a clearer picture, a parametric study was carried out varying fuselage mass and (pitching) moment of inertia. When pitching inertia was fixed, increasing fuselage mass was promoting a body freedom flutter (BFF). Conversely, fixing fuselage weight and varying moment of inertia showed an interesting scenario: for low pitching inertia BFF was the instability mechanism, accompanied by a coalescence of pitching and first elastic mode frequencies. As progressively increasing the inertia, the flutter speed associated with BFF progressively increased and the instability eventually disappeared. However, second mode instability was

experiencing the opposite trend. Thus, for a sufficiently large value of the inertia, the classic cantilever flutter, with a coalescence of first and second elastic modes' frequencies was recovered.

This effort represents a first step toward a complete free-flying trimmed analysis of a PrandtlPlane configuration.

IX. Acknowledgements

The authors acknowledge the support by San Diego State University (College of Engineering) and University of California San Diego (Graduate Student Association). They also like to warmly thank Professor Aldo Frediani of the Aerospace Engineering Department of Università di Pisa for his valuable suggestions and for providing us the original PrandtlPlane model, Professor Mark Voskuijl of the Aerospace Engineering Department of Delft Institute of Technology, Daan Van Ginneken and Nicolas Divoux for sharing their material and clarifying and summarizing their previous work, starting point for this effort.

A. Contribution of Freeplay Springs to the Tangent Matrix

It is necessary to recall few mathematical definitions which will be necessary to develop the spring's contribution to the tangent matrix:

- $\boldsymbol{U}$, called the *displacement array* refers to the generalized displacements. It is then an *array* with 3 translational and 3 rotational components for each node. Thus, for a model with N nodes, $\boldsymbol{U}$ has $6N$ components.
- $\boldsymbol{x}$ refers to the translational (cartesian) coordinates of a node.
- If $\boldsymbol{a}$ and $\boldsymbol{b}$ are arrays
$$\left[\frac{\mathrm{d}\boldsymbol{a}}{\mathrm{d}\boldsymbol{b}}\right]_{ij} = \frac{\mathrm{d}a_i}{\mathrm{d}b_j}$$
- If $\boldsymbol{a}$ and $\boldsymbol{b}$ are arrays, *dyadic operator* is defined as:
$$[\boldsymbol{a} \otimes \boldsymbol{b}]_{ij} = a_i b_j$$

The keypoint to asses the freeplay spring contributions to the tangent matrix consists in evaluating the derivatives of the spring reaction (not yet projected to the nodes) in respect of the nodal displacements, i.e:

$$\frac{\mathrm{d}(M\,\boldsymbol{e}^A)}{\mathrm{d}\boldsymbol{U}} = \underbrace{\boldsymbol{e}^A \otimes \frac{\mathrm{d}M}{\mathrm{d}\boldsymbol{U}}}_{\text{term1}} + \underbrace{M\frac{\mathrm{d}\boldsymbol{e}^A}{\mathrm{d}\boldsymbol{U}}}_{\text{term2}} \tag{3}$$

TERM1 The first term of eq.(3) is evaluated exploiting a chain rule, and evaluating the derivatives:

$$\text{term1} = \boldsymbol{e}^A \otimes \left(\frac{\mathrm{d}M}{\mathrm{d}\Delta\theta}\,\frac{\mathrm{d}\Delta\theta}{\mathrm{d}\boldsymbol{U}}\right) \tag{4}$$

The first term inside the parenthesis depends on the freeplay spring law relating the deflection and the reaction of the spring, $M = M(\Delta\theta)$. The last term depends on the expression of $\Delta\theta$ given in Eq.(2):

$$\text{term1b} = \frac{\mathrm{d}\Delta\theta}{\mathrm{d}\boldsymbol{U}} = \frac{\mathrm{d}}{\mathrm{d}\boldsymbol{U}}\left(\sin^{-1}(\underbrace{(\boldsymbol{n}^M \times \boldsymbol{n}^S)\cdot\boldsymbol{e}^A}_{y^*})\right) = \frac{1}{\sqrt{1-y^{*2}}}\frac{\mathrm{d}y^*}{\mathrm{d}\boldsymbol{U}} \tag{5}$$

where:

$$\frac{\mathrm{d}y^*}{\mathrm{d}U_i} = \left[\frac{\mathrm{d}\boldsymbol{n}^M}{\mathrm{d}U_i}\times\boldsymbol{n}^S + \boldsymbol{n}^M \times \frac{\mathrm{d}\boldsymbol{n}^S}{\mathrm{d}U_i}\right]\cdot\boldsymbol{e}^A + \left[\frac{\mathrm{d}\boldsymbol{e}^A}{\mathrm{d}U_i}\right]\cdot(\boldsymbol{n}^M\times\boldsymbol{n}^S) \tag{6}$$

To evaluate the derivatives of the element's normal, with reference to Fig. 45, it holds:

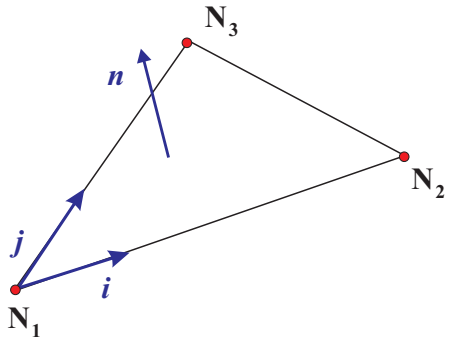

Fig. 45. Generic triangular finite element, nodes N_1, N_2, N_3, unit vectors i and j connecting the nodes as shown, and normal to the plane unit vector n.

$$\boldsymbol{n} = \frac{\boldsymbol{i} \times \boldsymbol{j}}{\|\boldsymbol{i} \times \boldsymbol{j}\|} \tag{7}$$

Considering the derivative of $\boldsymbol{n}$ in respect of the i-th component of the coordinate vector of node N_j (both $i, j = 1, 2, 3$), that is:

$$\frac{\partial \boldsymbol{k}}{\partial (\boldsymbol{x}^{N_j} \cdot \boldsymbol{e}_i)} = \frac{\partial \boldsymbol{k}}{\partial x_i^{N_j}} \tag{8}$$

where $\boldsymbol{e}_i$ represents the unit vector directed along the i-th cartesian component. By means of eq.(7) it is possible to demonstrate that:

$$\frac{\partial \boldsymbol{n}}{\partial x_i^{N_j}} = \left(\frac{\partial \boldsymbol{i}}{\partial x_i^{N_j}} \times \boldsymbol{j} + \boldsymbol{i} \times \frac{\partial \boldsymbol{j}}{\partial x_i^{N_j}} \right) \|\boldsymbol{i} \times \boldsymbol{j}\|^{-1} + \frac{(\boldsymbol{i} \times \boldsymbol{j})(\boldsymbol{i} \cdot \boldsymbol{j})}{\|\boldsymbol{i} \times \boldsymbol{j}\|^3} \left(\frac{\partial \boldsymbol{i}}{\partial x_i^{N_j}} \cdot \boldsymbol{j} + \boldsymbol{i} \cdot \frac{\partial \boldsymbol{j}}{\partial x_i^{N_j}} \right) \tag{9}$$

TERM2 The second term of eq.(3), enters also eq.(6). Hinge line direction is expressed by the unit vector defined as (see Fig. 1):

$$\boldsymbol{e}^A = \frac{\boldsymbol{x}^{H2} - \boldsymbol{x}^{H1}}{\|\boldsymbol{x}^{H2} - \boldsymbol{x}^{H1}\|} \tag{10}$$

After some calculations it is found that:

$$\frac{\partial \boldsymbol{e}^A}{\partial x_i^{Hj}} = \frac{\delta_{j2} - \delta_{j1}}{\|\boldsymbol{x}^{H2} - \boldsymbol{x}^{H1}\|} \left[\boldsymbol{e}_i + (\boldsymbol{e}^A \cdot \boldsymbol{e}_i)\, \boldsymbol{e}^A \right] \tag{11}$$

Once the expression of eq.(3) has been explicitated, the contribution to the tangent matrix can be easily assessed remembering to equally distribute the moment (with the appropriate sign) between the two hinge nodes on the master and slave elements.

References

[1]Wolkovitch, J., "The Joined Wing Aircraft: an Overview," *Journal of Aircraft*, Vol. 23, No. No. 3, March 1986, pp. 161–178.

[2]Chambers, J. R., *Innovation in Flight: Research of the NASA Langley Research Center on Revolutionary Advanced Concepts for Aeronautics*, No. 39 in Monograph in Aerospace History, NASA, November 2005, NASA SP 2005-4539.

[3]Rizzo, E., *Optimization Methods Applied to the preliminary design of innovative non conventional aircraft configurations*, Edizioni ETS.

[4]Rizzo, E. and Frediani, A., "Application of Optimisation Algorithms to Aircraft Aerodynamics," *Variational Analysis and Aerospace Engineering*, edited by G. Buttazzo and A. Frediani, Vol. 33 of *Springer Optimization and Its Applications*, Springer New York, 2009, pp. 419–446.

[5]Blair, M., Canfield, R. A., and Roberts Jr., R. W., "Joined-Wing Aeroelastic Design with Geometric Nonlinearity," *Journal of Aircraft*, Vol. 42, No. No. 4, July 2005, pp. 832–848.

[6]Demasi, L., Cavallaro, R., and Razón, A., "Postcritical Analysis of PrandtlPlane Joined-Wing Configurations," *AIAA Journal*, Vol. 51, No. 1, 2013, pp. 161–177.

[7]Cavallaro, R., Demasi, L., and Passariello, A., "Nonlinear Analysis of PrandtlPlane Joined Wings - Part II: Effects of Anisotropy," No. AIAA 2012-1462, 53rd AIAA/ASME/ASCE/AHS/ASC Structures, Structural Dynamics, and Materials Conference, Honolulu, Hawaii, 23-26 April 2012.

[8]Cavallaro, R., Demasi, L., Bertuccelli, F., and Benson, D. J., "Risks of Linear Design of Joined Wings: a Nonlinear Dynamic Perspective in the Presence of Follower Forces," *CEAS Aeronautical Journal*, November 2014, pp. 1–20.

[9]Demasi, L., Cavallaro, R., and Bertuccelli, F., "Post-Critical Analysis of Highly Deformable Joined Wings: the Concept of Snap-Divergence as a Characterization of the Instability," *Journal of Fluids and Structures*, 2015, In press.

[10]Demasi, L. and Palacios, A., "A Reduced Order Nonlinear Aeroelastic Analysis of Joined Wings Based on the Proper Orthogonal Decomposition," 2010, Presented at the 51st AIAA/ASME/ASCE/AHS/ASC Structures, Structural Dynamics & Materials Conference, Orlando, Florida, 12-15 April 2010.

[11]Demasi, L. and Livne, E., "The Structural Order Reduction Challenge in the Case of Geometrically Nonlinear Joined-Wing Configurations," 2007, Presented at the 48th AIAA/ASME/ASCE/AHS/ASC Structures, Structural Dynamics & Materials Conference, Honolulu, Hawaii, 23-26 April 2007.

[12]Teunisse, N., Tiso, P., Demasi, L., and Cavallaro, R., "A Computational Method for Structurally Nonlinear Joined Wings Based on Modal Derivatives," No. AIAA 2014-0494, 55th AIAA/ASMe/ASCE/AHS/SC Structures, Structural Dynamics, and Materials Conference, AIAA Science and Technology Forum and Exposition (SciTech2014) National Harbor, Maryland, American Institute of Aeronautics and Astronautics, 13-17 January 2014.

[13]Phlipot, G., Wang, X., Mignolet, M., Demasi, L., and Cavallaro, R., "Nonintrusive Reduced Order Modeling for the Nonlinear Geometric Response of Some Joined Wings," No. AIAA 2014-0151, 55th AIAA/ASMe/ASCE/AHS/SC Structures, Structural Dynamics, and Materials Conference, AIAA Science and Technology Forum and Exposition (SciTech2014) National Harbor, Maryland, American Institute of Aeronautics and Astronautics, 13-17 January 2014.

[14]Teunisse, N., Tiso, P., Demasi, L., and Cavallaro, R., "Reduced Order Methods and Algorithms for Structurally Nonlinear Joined Wings," 56th AIAA/ASMe/ASCE/AHS/SC Structures, Structural Dynamics, and Materials Conference, AIAA Science and Technology Forum and Exposition (SciTech2015) Kissimmee, Florida, 5-9 January 2015.

[15]Demasi, L., Cavallaro, R., and Bertuccelli, F., "Post-Critical Analysis of Joined Wings: the Concept of Snap-Divergence as a Characterization of the Instability," No. AIAA 2013-1559, 54th AIAA/ASME/ASCE/AHS/ASC Structures, Structural Dynamics, and Materials Conference, Boston, Massachusetts, American Institute of Aeronautics and Astronautics, 8-11 April 2013.

[16]Cavallaro, R., Iannelli, A., Demasi, L., and Razón, A. M., "Phenomenology of Nonlinear Aeroelastic Responses of Highly Deformable Joined Wings," *Advances in Aircraft and Spacecraft Science, An International Journal*, , No. AAS47174E, 2014, In press.

[17]Cavallaro, R., Iannelli, A., Demasi, L., and Razón, A. M., "Phenomenology of Nonlinear Aeroelastic Responses of Highly Deformable Joined-wings Configurations," No. AIAA 2014-1199, 55th AIAA/ASMe/ASCE/AHS/SC Structures, Structural Dynamics, and Materials Conference, AIAA Science and Technology Forum and Exposition (SciTech2014) National Harbor, Maryland, 13-17 January 2014.

[18]Divoux, N. and Frediani, A., "The Lifting System of a PrandtlPlane, Part 2: Preliminary Study on Flutter Characteristics," *Variational Analysis and Aerospace Engineering: Mathematical Challenges for Aerospace Design*, edited by G. Buttazzo and A. Frediani, Vol. 66 of *Springer Optimization and Its Applications*, Springer US, 2012, pp. 235–267, 10.1007/978-1-4614-2435-2_10.

[19]Dal Canto, D., Frediani, A., Ghiringhelli, G. L., and Terraneo, M., "The Lifting System of a PrandtlPlane, Part 1: Design and Analysis of a Light Alloy Structural Solution," *Variational Analysis and Aerospace Engineering: Mathematical Challenges for Aerospace Design*, edited by G. Buttazzo and A. Frediani, Vol. 66 of *Springer Optimization and Its Applications*, Springer US, 2012, pp. 211–234, 10.1007/978-1-4614-2435-2_9.

[20]Ginneken, D. A. J., Voskuijl, M., Van Tooren, M. J. L., and Frediani, A., "Automated Control Surface Design and Sizing for the PrandtlPlane," No. AIAA 2010-3060, 2010, Presented at the 51st AIAA/ASME/ASCE/AHS/ASC Structures, Structural Dynamics & Materials Conference, Orlando, Florida, 12-15 April 2010.

[21]Voskuijl, M., Klerk, J., and Ginneken, D., "Flight Mechanics Modeling of the PrandtlPlane for Conceptual and Preliminary Design," *Variational Analysis and Aerospace Engineering: Mathematical Challenges for Aerospace Design*, edited by G. Buttazzo and A. Frediani, Springer Optimization and Its Applications, Springer US, 2012, pp. 435–462.

[22]Miranda, L. R., "Boxplane Wing and Aircraft," September 1974.

[23]Frediani, A., "Swept-wing box-type aircraft with high flight static stability," Feb. 2004, WO Patent App. PCT/IT2004/000,071.

[24]Frediani, A., "New Large Aircraft," 2002, European Patent EP 0716978B1, 20 March 2002.

[25]Frediani, A., "Velivolo Biplano ad Ali Contrapposte," 2003, Italian Patent FI 2003A000043, 19 February 2003.

[26]Buttazzo, G. and Frediani, A., editors, *Variational Analysis and Aerospace Engineering: Mathematical Challenges for Aerospace Design Contributions from a Workshop held at the School of Mathematics in Erice, Italy*, Springer US, 2012.

[27]Bisplinghoff, R. and Ashley, H., *Principles of Aeroelasticity*, Dover Phoenix Editions, Dover Publications, 2002.

[28]Clark, R., Cox, D., Jr., H. C. C., Edwards, J. W., Hall, K. C., Peters, D. A., Scanlan, R., Simiu, E., Sisto, F., and Strganac, T. W., *A Modern Course in Aeroelasticity*, Vol. 116 of *Solid Mechanics and Its Applications*, Springer Netherlands, 2005.

[29]Dal Canto, D., *Progetto preliminare del cassone alare di un velivolo di tipo Prandtl-Plane mediante l'applicazione di un metodo di ottimizzazione strutturale*, Master's thesis, Dipartimento di Ingegneria Aerospaziale, Università di Pisa, December 2009, Advisor: Alfo Frediani.

[30]Divoux, N., *Preliminary Study on Flutter Characteristics of a PrandtlPlane Aircraft*, Master's thesis, TU Delft, 2008.

[31]Quattrone, F. and Contini, F., *Preliminary design and FEM analysis of a new conception non-standard wing structure: the PrandtlPlane 250 wing structure*, Master's thesis, Dipartimento di Ingegneria Aerospaziale, Università di Pisa, October 2010, Advisor: Alfo Frediani.

[32]Frediani, A., Quattrone, F., and Contini, F., "The Lifting System of a PrandtlPlane, Part 3: Structures Made in Composites," *Variational Analysis and Aerospace Engineering: Mathematical Challenges for Aerospace Design*, edited by G. Buttazzo and A. Frediani, Vol. 66 of *Springer Optimization and Its Applications*, Springer US, 2012, pp. 269–288, 10.1007/978-1-4614-2435-2_11.

[33]Dowell, E., Edwards, J., and Strganac, T., "Nonlinear Aeroelasticity," *Journal of Aircraft*, Vol. 40, No. 5, September 2003, pp. 857–874.

[34]Tang, D. and Dowell, E. H., "Flutter and Limit-Cycle Oscillations for a Wing-Store Model with Freeplay," *Journal of Aircraft*, Vol. 43, No. 2, 2006, pp. 487–503.

[35]Ginneken, D. V., *Automated Control Surface Design and Sizing for the PrandtlPlane*, Master's thesis, TU Delft, April 2009.

[36]Lange, R. H., Cahill, J. F., Bradley, E. S., Eudaily, R. R., Jenness, C. M., and Macwilkinson, D. G., "Feasibility Study of the Transonic Biplane Concept for Transport Aircraft Applications," 1974, NASA CR–132462, Lockheed–Georgia Company.

[37]Weisshaar, T. A. and Lee, D. H., "Aeroelastic Tailoring of Joined-Wing Configurations," 43nd AIAA/ASME/ASCE/AHS/ASC Structures, Structural Dynamics and Materials Conference, Denver, CO,, 22-25 April 2002.

[38]Cavallaro, R., Demasi, L., and Passariello, A., "Nonlinear Analysis of PrandtlPlane Joined Wings: Effects of Anisotropy," *AIAA Journal*, Vol. 52, No. 5, May 2014, pp. 964–980.

[39]Gordnier, R. E. and Melville, R. B., "Numerical Simulation of Limit-cycle Oscillations of a Cropped Delta Wing Using the Full Navier-Stokes Equations," *International Journal of Computational Fluid Dynamics*, Vol. 14, No. 3, 2001, pp. 211–224.

[40]Gordnier, R. E., "Computation of Limit-Cycle Oscillations of a Delta Wing," *Journal of Aircraft*, Vol. 40, No. 6, 2003, pp. 1206–1208.

[41]Attar, P. and Gordnier, R., "Aeroelastic prediction of the limit cycle oscillations of a cropped delta wing," *Journal of Fluids and Structures*, Vol. 22, No. 1, 2006, pp. 45 – 58.

[42]Levy, R. and Gal, E., "Triangular Shell Element for Large Rotations Analysis," *AIAA Journal*, Vol. 41, No. No. 12, December 2003, pp. 2505–2508.

[43]Levy, R. and Spillers, W., *Analysis of geometrically nonlinear structures*, No. v. 1, Kluwer Academic Publishers, 2003.

[44]Gal, E. and Levy, R., "The Geometric Stiffness of Triangular Composite-Materials Shell Elements," *Computers and Structures*, Vol. 83, 2005, pp. 2318–2333.

[45]Gal, E., Levy, R., Abramovich, H., and Pavsner, P., "Buckling analysis of composite panels," *Composite Structures*, Vol. 73, No. 2, 2006, pp. 179 – 185, International Conference on Buckling and Postbuckling Behavior of Composite Laminated Shell Structures.

[46]Liu, L. and Dowell, E. H., "Harmonic Balance Approach for an Airfoil with a Freeplay Control Surface," *AIAA journal*, Vol. 43, No. 4, April 2005, pp. 802–815.

[47]Rodden, W. P. and Johnson, E. H., *User Guide V 68 MSC/NASTRAN Aeroelastic Analysis*, MacNeal-Schwendler Corporation, 1994.

[48]Katz, J. and Plotkin, A., *Low-Speed Aerodynamics*, Cambridge Aerospace Series, Cambridge University Press, 2001.

[49]Quaranta, G., Masarati, P., and Mantegazza, P., "A conservative mesh-free approach for fluid structure problems in Coupled Problems," *International Conference for Coupled Problems in Science and Engineering, Santorini, Greece*, 23-29 May 2005, pp. 24–27.

[50]Karaağaçli, T., Yildiz, E. N., and Özgüven, H. N., "Determination of Dynamically Equivalent FE Models of Structures from Experimental Data," *Structural Dynamics, Volume 3*, edited by T. Proulx, Conference Proceedings of the Society for Experimental Mechanics Series, Springer New York, 2011, pp. 785–799.

[51]Blair, M., Garmann, D., Canfield, R., Bond, V., Pereira, P., and Suleman, A., "Non-Linear Aeroelastic Scaling of a Joined-Wing Concept," No. AIAA 2007-1887, 48th AIAA/ASME/ASCE/AHS/ASC Structures, Structural Dynamics, and Materials Conference, Honolulu, Hawaii, 23-26 April 2007.

[52]Ricciardi, A. P., Eger, C. A. G., Canfield, R. A., and Patil, M. J., "Nonlinear Aeroelastic-Scaled-Model Optimization Using Equivalent Static Loads," *Journal of Aicraft*, 2014.

[53]Addis, B., Locatelli, M., and Schoen, F., "Local Optima Smoothing for Global Optimization," *OPTIMIZATION METHODS AND SOFTWARE*, Vol. 20, 2005, pp. 437.

[54]Torenbeek, E., *Synthesis of Subsonic Airplane Design: An Introduction to the Preliminary Design of Subsonic General Aviation and Transport Aircraft, with Emphasis on Layout, Aerodynamic Design, Propulsion and Performance*, Springer, 1982.

[55]Bramesfeld, G., *A Higher Order Vortex-Lattice Method with a Force-Free Wake*, Ph.D. thesis, The Pennsylvania State University, August 2006.

[56]Bansal, P. and Pitt, D. M., "Uncertainties in control surface free-play and structural properties and their effect on flutter and LCO," No. AIAA 2014-0679, 55th AIAA/ASMe/ASCE/AHS/SC Structures, Structural Dynamics, and Materials Conference, AIAA Science and Technology Forum and Exposition (SciTech2014) National Harbor, Maryland, 13-17 January 2014.

[57]Theodorsen, T. and Garrick, I. E., "Flutter calculations in three degrees of freedom," naca-report-741, NACA, 1942.

[58]Love, M. H., Zink, P. S., Wieselmann, P. A., and Youngren, H., "Body Freedom Flutter of High Aspect Ratio Flying Wings," No. AIAA 2005-1947, 46th AIAA/ASME/ASCE/AHS/ASC Structures, Structural Dynamics and MMaterial Conference, Austin, Texas, 18-21 April 2005.

[59]Lambourne, N., "An Experimental Investigation on the Flutter Characteristics of a Model Flying Wing," Aeronautical Research Council. Reports and Memoranda. No. 2626, 1952.

[60]Chipman, R., Rauch, F., Rimer, M., and Muñiz, B., "Body-freedom Flutter of a 1/2 Scale Forward-Swept-Wing Model, an Experimentwal and Analytical Study," Contract Report NASA CR-172324, NASA, April 1984, by Grumman Aerospace Corporation.

[61]Reichenbach, E., "Aeroservoelastic Design and Test Validation of the Joined Wing Sensorcraft," No. AIAA 2008-7189, 26th AIAA Applied Aerodynamics Conference, Honolulu, Hawaii, 18-21 August 2008.

[62]Livne, E. and Weisshaar, T. A., "Aeroelasticity of Nonconventional Airplane Configurations-Past and Future," *Journal of Aircraft*, Vol. 40, No. No. 6, November 2003, pp. 1047–1065.

[63]Dimartino, C. and Baldini, M., *Analisi agli elementi finiti di un tronco di fusoliera di un velivolo PrandtlPlane sottoposto a carichi limite di pressurizzazione e di massa.*, Master's thesis, Università di Pisa, 2009.

[64]Frediani, A., Rizzo, E., Bottoni, C., Scanu, J., and Iezzi, G., "A 250 Passenger PrandtlPlane Transport Aircraft Preliminary Design," *Aerotecnica Missili e Spazio (AIDAA)*, Vol. 84, 2005.